Contrib Mineral Petrol (2000) 140: 363–381

Igor M. Villa · Jörg Hermann · Othmar Müntener
Volkmar Trommsdorff

^{39}Ar–^{40}Ar dating of multiply zoned amphibole generations (Malenco, Italian Alps)

Received: 1 March 1999 / Accepted: 18 August 2000

Abstract Mafic rocks of a Permian crust to mantle section in Val Malenco (Italy) display a multi-stage evolution: pre-Alpine exhumation to the ocean floor, followed by burial and re-exhumation during Alpine convergence. Four prominent generations of amphiboles were formed during these stages. On the basis of microstructural investigations combined with electron microprobe analyses two amphibole generations can be assigned to the pre-Alpine decompression and two to the Alpine metamorphic P–T evolution. The different amphiboles have distinct Na^{M4}, Ca, K and Cl contents according to different P–T conditions and fluid chemistry. Analysing these mixed amphiboles by the ^{39}Ar–^{40}Ar stepwise heating technique yielded very complex age spectra. However, by correlating amphibole compositions directly obtained from the electron microprobe with the components deduced from the release of Ar isotopes during stepwise heating, obtained ages were consistent with the geological history deduced from field and petrological studies. The two generations of pre-Alpine amphiboles gave distinguishable Triassic to Late Jurassic/Early Cretaceous ages (≈225 and 130–140 Ma respectively). High-Na^{M4} amphiboles have higher isotopic ages than low-Na^{M4} ones, in agreement with their decompressional evolution. The exhumation of the Permian crust to mantle section is represented by the former age. The latter age concerns Cl-dominated amphibole related to an Early Cretaceous oceanic stage. For the early Alpine, pressure-dominated metamorphism we obtained a Late Cretaceous age (83–91 Ma). The later, temperature-dominated overprint is significantly younger, as indicated by ^{39}Ar–^{40}Ar ages of 67–73 Ma. These Late Cretaceous ages favour an Adriatic origin for the Malenco unit. Our data show that ^{39}Ar–^{40}Ar dating combined with detailed microprobe analysis can exploit the potential to relate conditions of amphibole formation to their respective ages.

I. M. Villa (✉)
Isotopengeologie, Erlachstrasse 9a, 3012 Bern, Switzerland
e-mail: igor@mpi.unibe.ch
Tel.: +41-31-6318777; Fax: +41-31-6314988

J. Hermann · O. Müntener · V. Trommsdorff
Institut für Mineralogie und Petrographie,
ETH Zürich, 8092 Zürich, Switzerland

Editorial responsibility: J. Hoefs

Introduction

In many metamorphic rocks, "minerals" consist of multiple generations formed at different times with different chemical compositions. Electron microscopy has shown in recent years that intergrowths of multiple generations are ubiquitous, usually at the sub-micrometre scale (Livi and Veblen 1987; Veblen 1992; Parsons et al. 1999). In view of these mineralogical complexities, it might be necessary to question the assumption of simple, homogeneous minerals on which geochronology was based.

Multi-chronometric investigations are hampered by the fact that most isotopic methods are capable of dating bulk minerals only, which reduces the information that can be obtained from polymetamorphic rocks. Only dating methods that allow insight into intra-mineral isotopic heterogeneities may be useful in such cases. Yet ^{39}Ar–^{40}Ar dating of mineral mixtures is generally not considered productive, because mixtures often result in irregular age spectra.

Turner et al. (1971) were first to realize that whole rocks showed a correlation between Ca/K ratio and ^{39}Ar–^{40}Ar step ages because they reflected polymineralic assemblages. However, in the following years, no practical way of disentangling the age spectra was proposed, and the occurrence of mineral mixtures was considered to prevent the reconstruction of geological histories. Only in the very recent past has it become possible to

We follow the convention of all other isotopic systems and denote the dating method in the order parent–daughter.

estimate ages for the components of the mixing. This approach makes use of suitable Ar isotope correlation diagrams to recognize mineral mixtures (Villa et al. 1996a, b, 1997; Boriani and Villa 1997). Three-isotope correlation diagrams are a prime tool allowing identification of separate rare gas components (Hohenberg et al. 1967); these components have generally been viewed as physically distinct reservoirs. With the help of the electron microprobe (EMP) it is then possible to test for the existence of such inferred, chemically and mineralogically resolvable entities.

Amphibole has been widely recognized as a monitor of polyphase metamorphic evolutions (Raase 1974; Laird and Albee 1981) due to its compositional sensitivity to changing pressure, temperature and bulk rock composition. The variety of amphiboles is such that a small difference in the P–T conditions of amphibole formation will result in a detectable chemical difference between successive amphibole generations. Amphiboles, on the other hand, are quite stable once formed, and it is a common microstructural observation that amphiboles overgrow, without necessarily substituting, one another. The diffusivity of structure-forming ions appears to be negligible compared to the effects of new crystallization. The diffusivity of trace radiogenic daughters has been recently reassessed; the diffusion coefficients for doubly charged Sr and for neutral Ar are identical (Brabander and Giletti 1995; Villa et al. 1996b). Atoms of trace elements having either a high charge (such as Sr) or a large radius (such as Ar) cannot move out of the unit cell they occupy unless the mineral structure forms vacancies. For example, Ar cannot diffuse faster than the structure-forming Al and Si exchange in sanidine (Nyfeler et al. 1998). In the case of amphiboles, comparison of Sr and Ar diffusivities (Brabander and Giletti 1995; Villa et al. 1996b) strongly suggests the same to be the case: Ar is not lost from an amphibole unless its structure-forming cations also moved. Therefore, it is plausible that minor elements or radiogenic isotopes preserve the record of the conditions under which their host amphibole was formed. If an amphibole is observed to be chemically homogeneous, this is taken to mean that it did not change its composition by diffusion of elements including Ar.

In the present work we describe how to unravel the geochronological information hidden in a heterogeneous, polyphasic amphibole. In order to do so, we selected a sample suite for which the chronological evolution was already known, albeit broadly. In the Malenco unit (Fig. 1) geological and petrological constraints exist that permit an independent control of the

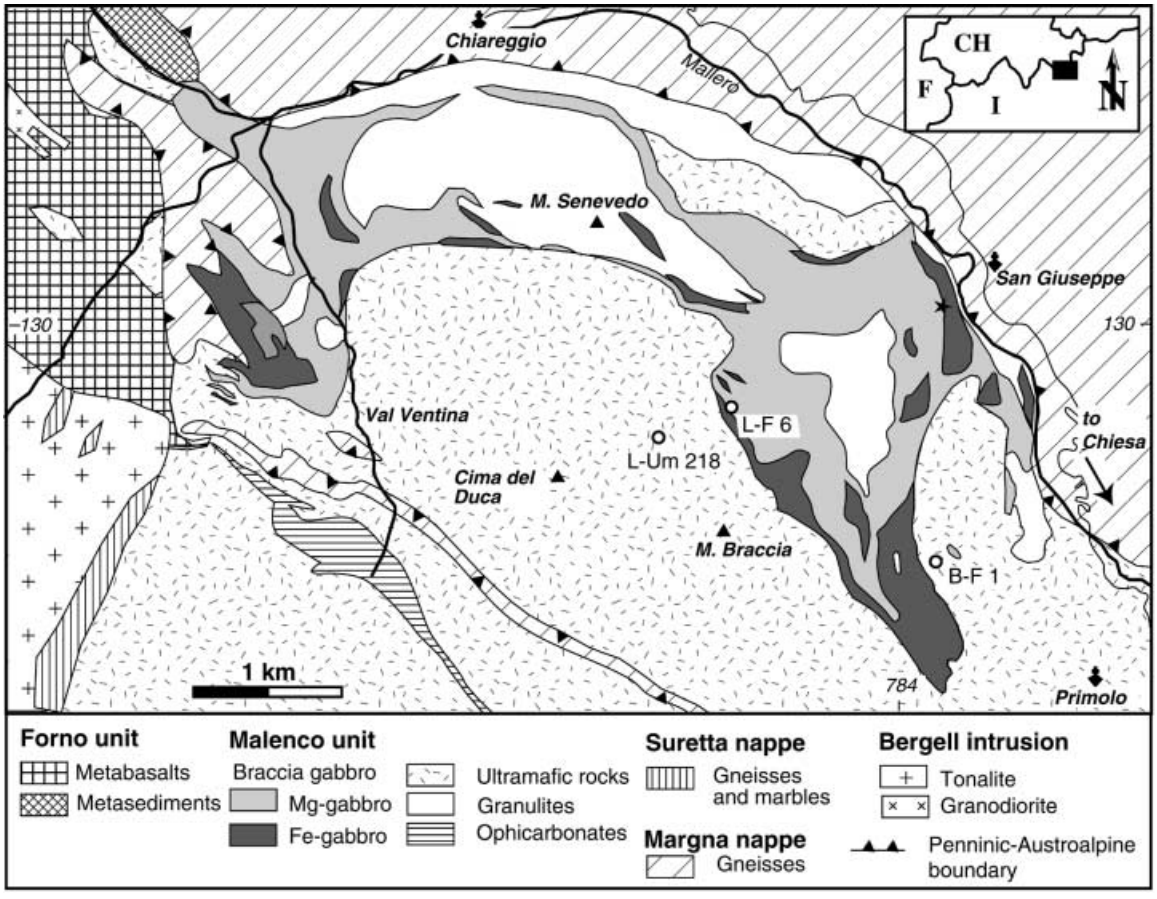

Fig. 1 Geological map of the Val Malenco area with sample locations. For a detailed geological map and description of rock types, see Müntener and Hermann (1996)

inferences of our geochronological study. Our aim was twofold: firstly, to attempt to refine the chronological constraints on the metamorphic evolution of the Malenco unit; secondly, to use the exceptionally well-defined geological framework to understand to what extent the pre-Alpine record was preserved in these polymetamorphic rocks. For both aims it is necessary to combine the ^{39}Ar–^{40}Ar stepwise heating technique on hand-picked amphiboles with detailed microchemical investigations on the mineral separate.

Geological constraints

The Malenco unit, situated at the Penninic–Austroalpine boundary in the Val Malenco (N Italy, Alps; Fig. 1), formed a crust-to-mantle transition in Permian times. A gabbro intruded the lithospheric mantle as well as the lowermost continental crust at 35 km depth (Trommsdorff et al. 1993; Müntener and Hermann 1996; Hermann et al. 1997). U–Pb age determinations on zircons yield a Permian age of 270 + 6/−4 Ma for the gabbro intrusion (Hansmann et al. 1996).

The pre-Alpine P–T evolution and subsequent exhumation has been discussed by Müntener et al. (2000) and is sketched here in Fig. 2. Firstly, the rocks underwent anhydrous recrystallization and cooled from 800 °C down to 600 °C with moderate decompression from 1.0–0.85 GPa. Then, a near-isothermal decompression is documented by hydrous parageneses. Amphiboles formed during decompression display a decrease in Na^{M4} content (Hermann 1997; Müntener 1997). Serpentinization of ultramafic rocks, concomitant rodingitization of ultramafic–mafic contacts, and formation of ophicarbonates (Fig. 1) provide evidence of subsequent exhumation to the ocean floor (Trommsdorff et al. 1993). Stable isotope results (Burkhart and O'Neill 1988; Pozzorini and Früh-Green 1996) further support oceanic serpentinization. The mantle rocks are crosscut by MOR-type basalts of the Forno unit (Fig. 1), which are overlain by sediments that correlate well with Jurassic sequences (Peretti 1985; Weissert and Bernoulli 1985). On the basis

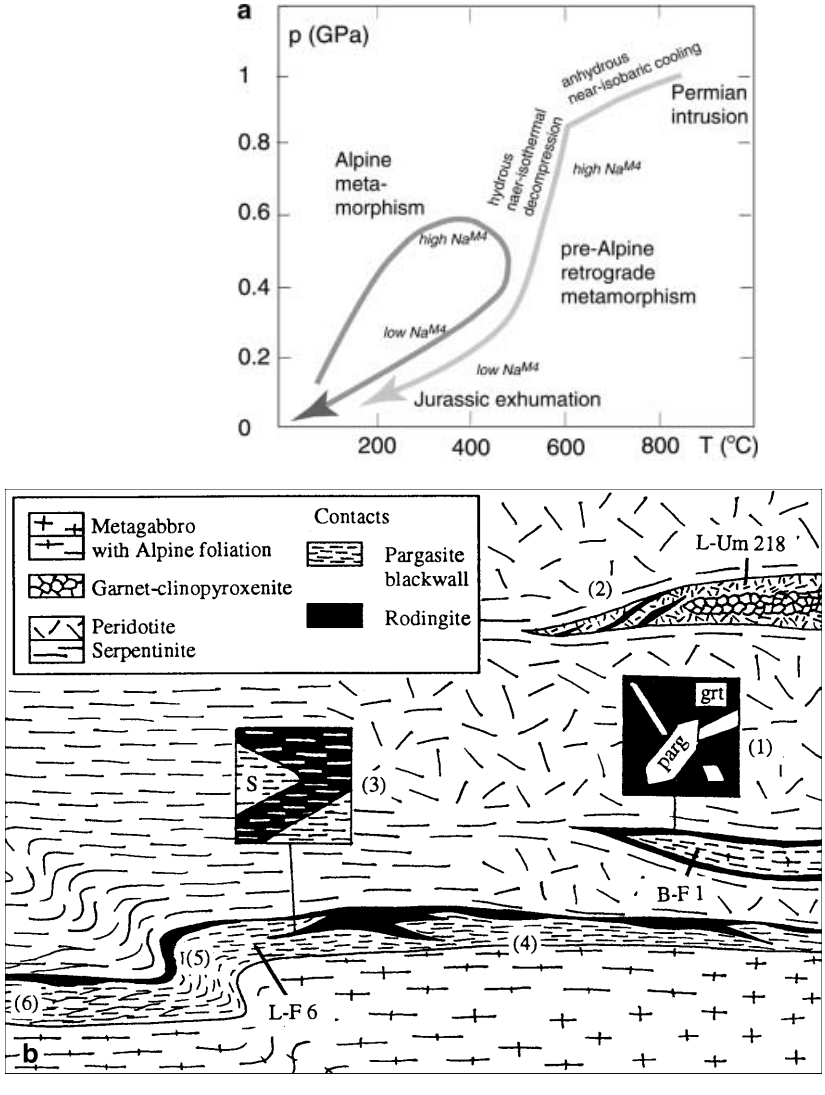

Fig. 2a P–T-age constraints on the evolution of the Malenco lower crust – upper mantle complex (after Müntener et al. 2000). Characteristics of amphiboles formed during this evolution are given in *italics*. **b** Schematic field relations of pargasite blackwalls (not to scale). Blackwalls formed at the contact between mafic and ultramafic rocks. Rodingites formed during metasomatism near the ocean floor and partly recrystallized during Alpine metamorphism. The degree of Alpine overprint increases from the *upper right* to the *lower left* corner. The positions of the dated samples are indicated. *Numbers* refer to the sample description in the text. *S* Alpine schistosity, *parg* pargasite, *grt* garnet

of this combined geological evidence, Trommsdorff et al. (1993) suggested that the Malenco rocks formed part of the Tethyan ocean floor in Jurassic times. To explain the exhumation of rocks originating from 30 km depth, large-scale extension has been considered. Extensional tectonics are well documented in Jurassic syn-rift sediments in the Austroalpine units (Froitzheim and Eberli 1990). The onset of Jurassic rifting has been proposed by Müntener et al. (2000) as the cause of near-isothermal decompression of the Malenco rocks.

During the subsequent Alpine cycle, the rocks of the Malenco unit were metamorphosed under epidote–amphibolite facies conditions. The pressure peak of 0.4–0.7 GPa inferred from Na^{M4} in amphiboles (Bissig and Hermann 1999) was followed by peak temperatures around 450 °C as determined by calcite–dolomite thermometry (Trommsdorff and Evans 1977; Mellini et al. 1987) and garnet–amphibole thermometry (Hermann 1997). The metamorphic pressures and temperatures are thus very similar to those in the overlying Margna nappe (Guntli and Liniger 1989; Bissig and Hermann 1999).

In summary, tight geological constraints exist in terms of the evolution between the Permian and the Cretaceous. There is a lack of precise geochronology of the metamorphic evolution: blackwalls (rocks at the contact between ultramafic and mafic ones, consisting predominantly of amphibole and chlorite) are almost monomineralic and contain no other unaltered mineral to use in a two-point isochron (e.g. Rb–Sr). Moreover, bulk analyses (such as Rb–Sr or conventional U–Pb) are clearly meaningless to date polymetamorphic minerals.

Sample description

Blackwalls consisting of about 90% pargasitic amphiboles, with minor zoisite, chlorite and diopside, formed at the contact between mafic and ultramafic rocks. On the basis of field and microscope observations, different pargasite generations are recognized (Fig. 2b). The oldest pargasite pre-dates rodingitization, as it occurs as inclusions in grossular and because rodingite veins cut pargasite-bearing rocks (1, 2 in Fig. 2b). It formed coevally with an early hydration of ultramafic–mafic contacts during pre-Alpine exhumation (Fig. 2a). A pre-Alpine origin of the blackwalls is further supported by the first Alpine foliation which in places deforms rodingite–blackwall contacts (3 in Fig. 2b). In most cases, however, pargasite recrystallized along the main Alpine foliation (3, 4 in Fig. 2b). Late recrystallization is documented by pargasites formed within the axial plane surface of late-stage folds (5 in Fig. 2b) and in pargasites forming shear bands (6 in Fig. 2b).

The three samples used for ^{39}Ar–^{40}Ar dating were collected in areas with different degrees of Alpine overprint (Fig. 2b). Sample locations and characterizations are given in Table 1. Sample L-UM 218 comes from a garnet–clinopyroxenite that was partly replaced by pargasite. The surrounding ultramafic rocks are metaperidotites with little Alpine metamorphic overprint. Sample B-F 1 was collected from a gabbro dyke within a partly serpentinized dunite. Pargasite is aligned within the Alpine foliation, providing evidence for Alpine recrystallization. Pre-Alpine pargasite is rare and enclosed in rodingitic garnet. Sample L-F 6 derives from a pervasively foliated and recrystallized blackwall between metagabbros and serpentinites which preserves no pre-Alpine relics.

Analytical techniques

The rocks were crushed and sieved. Amphiboles between 0.125 and 0.25 mm were enriched by magnetic and gravimetric means. Prolonged hand-picking of the separate led to a visual purity $>99.5\%$.

Electron microprobe

The separated minerals were mounted in epoxy resin and polished. Additionally, polished thin sections of the samples were used. Mineral compositions were analysed using a Cameca SX-50 microprobe, equipped with five crystal spectrometers. Samples were coated with 200 Å of carbon. Operating parameters include an acceleration potential of 15 kV, a beam current of 20 nA and a beam size of ~1 μm. The volume excited by the electron beam was approximately a 5-μm-diameter spheroid. Data collection on background positions on both sides of the peaks was half the time of data collection on the

Table 1 Sample location (with Swiss grid coordinates) and short description of assemblage accompanying the pargasites

Sample	Macro- and microscopic description of assemblage accompanying the pargasites
L-UM 218, Val Orsera, 781′130/128′600	Amphibolitized garnet–pyroxenite dyke within partly serpentinized peridotite Pargasite forms ~90% of the matrix, minor relics of clinopyroxene and garnet Pargasite overgrows statically the pyroxenite texture
B-F 1, Val Füraas, 784′250/128′400	Central part of a partly rodingitized gabbroic dyke cutting the ultramafic rocks Mg-pargasite coexists with clinozoisite, has small clinopyroxene inclusions Mg-pargasite replaces pyroxene and forms a weak foliation
L-F 6, Lagazzuolo, 782′750/129′480	Pargasitic blackwall in Fe-gabbro 1 m away from contact to ultramafic rocks Fe-pargasite coexists with titanite and apatite Fe-pargasite oriented along main schistosity, few postkinematic grains

respective peak position. Natural and synthetic oxides and silicates were used as standards. Counting time on peaks was generally 20 s, except Na (10 s), Ni (40 s) and Cl (60 s). Raw data were corrected for drift, dead time and background. A ZAF-type correction procedure was applied to the data (Pouchon and Pichoir 1984).

^{39}Ar–^{40}Ar stepwise heating

^{39}Ar–^{40}Ar analyses were performed in an all-metal extraction system containing a double-vacuum resistance oven with an external thermocouple. Typical steps lasted 20 min; the crucible was not cooled between steps. Of some relevance to the present paper is the temperature control: it is both known from the literature (Foland et al. 1993) and very easily directly controlled by melting-point calibrations and optical pyrometry that double-vacuum furnace thermocouples read outside temperatures which can be too high by 100 K compared to those in the crucible, whereby the temperature difference becomes smaller at high temperatures because of Stefan–Boltzmann's law. While our absolute T values are therefore probably no better known that ±30 K, the intra-sample relative temperature differences are likely to be better controlled than ±5 K, and inter-sample comparisons than ±2 K, as all samples were measured in immediate succession and crucible and resistance conditions were practically unchanged.

Samples were irradiated at the Risø research reactor (DK). Ar isotope analyses were performed on a MAP^{TM} 215–50B rare gas mass spectrometer. All isotopes were measured on the Faraday collector. Data listed in Table 2 were corrected for mass spectrometer back-

Table 2 Ar–Ar stepwise heating results. All Ar concentrations are in picolitres per gram (pl/g). Errors are 1 sigma. Ar* denotes total ^{40}Ar minus atmospheric ^{40}Ar; the integrated K_2O and CaO values are given in wt%; Cl is given in ppm. These values are calculated from the total ^{39}Ar, ^{37}Ar and ^{38}Ar, the production ratios and the irradiation time. Ages are given in Ma

Step	T (°C)	$^{40}Ar_{tot}$	^{39}Ar	^{38}Ar	^{37}Ar	^{36}Ar	Age ± 1σ
L-UM 218 (50.0 mg; J = 1.876 * 10^{-3}; Ar* = 684; K_2O = 0.16; CaO = 9.9; Cl = 1077)							
1	856	563.81 ± 0.04	0.117 ± 0.005	0.728 ± 0.004	4.56 ± 0.02	1.814 ± 0.009	688 ± 56
2	1034	112.75 ± 0.01	0.232 ± 0.006	0.554 ± 0.004	6.67 ± 0.02	0.332 ± 0.004	211 ± 16
3	1089	231.80 ± 0.02	3.998 ± 0.006	8.396 ± 0.016	105.64 ± 0.28	0.437 ± 0.003	92.8 ± 0.7
4	1124	152.17 ± 0.03	2.551 ± 0.006	6.056 ± 0.012	66.55 ± 0.18	0.290 ± 0.003	93.7 ± 1.2
5	1140	121.38 ± 0.01	2.041 ± 0.005	5.188 ± 0.013	53.06 ± 0.14	0.245 ± 0.003	86.9 ± 1.5
6	1156	127.73 ± 0.02	2.157 ± 0.006	5.671 ± 0.011	56.65 ± 0.15	0.246 ± 0.004	91.9 ± 1.7
7	1184	100.32 ± 0.01	1.369 ± 0.006	3.712 ± 0.008	36.15 ± 0.10	0.200 ± 0.004	107 ± 2.8
8	1219	125.26 ± 0.03	1.010 ± 0.005	2.739 ± 0.009	26.44 ± 0.07	0.285 ± 0.006	140 ± 5.0
9	1248	78.16 ± 0.02	0.494 ± 0.005	1.323 ± 0.007	13.98 ± 0.04	0.206 ± 0.005	123 ± 8.8
10	1322	199.45 ± 0.03	1.644 ± 0.006	4.544 ± 0.010	48.06 ± 0.13	0.386 ± 0.005	178 ± 2.5
11	1348	171.05 ± 0.02	1.219 ± 0.007	3.476 ± 0.011	39.51 ± 0.11	0.350 ± 0.004	190 ± 3.0
12	1488	181.35 ± 0.01	1.173 ± 0.007	3.195 ± 0.009	39.02 ± 0.10	0.348 ± 0.004	226 ± 3.2
B-F 1 (34.02 mg; J = 1.871 * 10^{-3}; Ar* = 946; K_2O = 0.36; CaO = 9.5; Cl = 21)							
1	852	634.11 ± 0.05	0.153 ± 0.004	0.589 ± 0.009	5.03 ± 0.02	2.011 ± 0.009	742 ± 42
2	1032	263.31 ± 0.04	0.135 ± 0.007	0.186 ± 0.003	4.32 ± 0.02	0.880 ± 0.009	87 ± 63
3	1090	271.86 ± 0.04	3.247 ± 0.007	0.168 ± 0.009	41.03 ± 0.11	0.670 ± 0.007	76.3 ± 2.1
4	1120	202.75 ± 0.04	2.574 ± 0.005	0.198 ± 0.006	31.53 ± 0.09	0.497 ± 0.007	72.5 ± 3.0
5	1141	230.56 ± 0.01	3.349 ± 0.007	0.152 ± 0.004	40.14 ± 0.11	0.520 ± 0.006	73.1 ± 3.1
6	1160	308.14 ± 0.03	4.608 ± 0.009	0.266 ± 0.009	52.82 ± 0.15	0.713 ± 0.005	73.2 ± 0.9
7	1178	309.26 ± 0.03	4.742 ± 0.009	0.232 ± 0.011	54.53 ± 0.15	0.660 ± 0.005	82.8 ± 1.0
8	1195	290.33 ± 0.03	4.451 ± 0.009	0.266 ± 0.010	50.77 ± 0.14	0.665 ± 0.007	73.0 ± 1.4
9	1226	399.09 ± 0.04	9.158 ± 0.011	0.324 ± 0.010	105.12 ± 0.28	0.645 ± 0.008	78.5 ± 0.8
10	1258	209.48 ± 0.03	1.469 ± 0.005	0.135 ± 0.009	19.59 ± 0.06	0.547 ± 0.008	111 ± 5.1
11	1325	264.79 ± 0.04	1.928 ± 0.007	0.213 ± 0.004	29.60 ± 0.08	0.740 ± 0.004	90.9 ± 2.0
12	1384	232.38 ± 0.02	1.718 ± 0.005	0.240 ± 0.012	25.93 ± 0.07	0.610 ± 0.005	104 ± 2.6
13	1491	240.91 ± 0.06	1.733 ± 0.006	0.212 ± 0.010	27.00 ± 0.08	0.667 ± 0.004	83.6 ± 2.3
L-F 6 (55.13 mg; J = 1.869 * 10^{-3}; Ar* = 1038; K_2O = 0.52; CaO = 10.1; Cl = 24)							
1	850	263.16 ± .03	0.646 ± 0.003	0.284 ± 0.007	3.05 ± 0.02	0.816 ± 0.005	112.9 ± 7.5
2	1033	104.81 ± 0.01	1.191 ± 0.004	0.087 ± 0.003	3.34 ± 0.03	0.296 ± 0.004	49.3 ± 2.8
3	1090	209.13 ± 0.05	9.020 ± 0.011	0.324 ± 0.006	93.62 ± 0.25	0.203 ± 0.001	57.7 ± 0.2
4	1120	113.68 ± 0.02	4.428 ± 0.007	0.135 ± 0.005	48.16 ± 0.13	0.146 ± 0.002	55.8 ± 0.3
5	1140	124.05 ± 0.02	5.036 ± 0.006	0.165 ± 0.006	51.00 ± 0.14	0.148 ± 0.003	55.7 ± 0.6
6	1176	235.94 ± 0.01	10.355 ± 0.011	0.296 ± 0.003	104.02 ± 0.28	0.160 ± 0.002	63.1 ± 0.2
7	1206	299.75 ± 0.02	12.680 ± 0.012	0.328 ± 0.004	121.70 ± 0.32	0.176 ± 0.002	67.3 ± 0.2
8	1239	92.48 ± 0.01	2.531 ± 0.005	0.105 ± 0.003	27.14 ± 0.07	0.144 ± 0.001	68.1 ± 0.5
9	1281	124.36 ± 0.01	4.118 ± 0.007	0.118 ± 0.003	47.85 ± 0.15	0.127 ± 0.005	73.0 ± 1.1
10	1321	123.74 ± 0.01	3.947 ± 0.008	0.137 ± 0.004	50.27 ± 0.14	0.179 ± 0.002	63.1 ± 0.5
11	1387	68.25 ± 0.01	1.255 ± 0.003	0.067 ± 0.005	16.06 ± 0.05	0.152 ± 0.004	65.0 ± 2.6
12	1490	86.90 ± 0.02	1.841 ± 0.005	0.111 ± 0.006	21.62 ± 0.06	0.188 ± 0.004	59.7 ± 1.9

ground (0.5 ± 0.15 fL for masses 36, 37 and 39) and discrimination (0.13%/amu favouring heavy masses, determined by a micropipette open to atmosphere). Furnace blanks always had atmospheric composition and ranged from 0.2 pL at 1000 °C to 0.5 pL at 1400 °C; they contained no detectable ^{37}Ar at any temperature. The dataset in Table 2 is complete and additional information [e.g. radiogenic ^{40}Ar ($^{40}Ar^*$) concentrations, Cl/Ca and $^{40}Ar^*/^{40}Ar_{tot}$ ratios, etc.] can be easily derived. The interference factors were: $(^{39}Ar/^{37}Ar)_{Ca} = 0.00067$; $(^{38}Ar/^{37}Ar)_{Ca} = 0.00023$; $(^{36}Ar/^{37}Ar)_{Ca} = 0.000255$; $(^{40}Ar/^{39}Ar)_K = 0.011$; $(^{38}Ar/^{39}Ar)_K = 0.0118$. Errors in Table 2 are in-run statistics only (with assigned uncertainties of 0.35% on discrimination and 1.5–3% on interference corrections) and purposefully do not take into account uncertainties on J gradient, monitor age and decay constants, which all affect all steps in the same way and therefore potentially mask the significance of inter-step age differences. The combined uncertainties on these are about 1.5% (Renne et al. 1998). The age monitor was the originally distributed MMhb-1, with an age of 523.1 Ma (Renne et al. 1998). We used the production rates from Ca and Cl calculated by Onstott et al. (1995).

Modelling the degassing behaviour of polymineralic aggregates

A major problem is the discordant and irregular amphibole age spectra (Figs. 4, 6, 7). In general, such spectra cannot be interpreted by the conventional approach which assumes that "the method relies upon the release of the Ar by thermal diffusion" (McDougall and Harrison 1988, p. 12) and that hornblendes "preserve and later reveal diffusion gradients" (McDougall and Harrison 1988, p. 113). It was therefore conventionally believed that age spectra mirrored a spatial "concentration profile" (McDougall and Harrison 1988, p. 106). Internally discordant age spectra are interpreted as contaminated by excess Ar and usually not discussed further. Recently, an alternative approach has been proposed, which takes into account both mineralogy and differential breakdown during laboratory degassing (Villa et al. 1996a, b). As our amphiboles exhibit overgrowth of several generations (Fig. 5), this approach has been further extended and is described below. It is important to point out that the scale of the overgrowths limits the analytical techniques that can be successfully used to unravel them. In order to achieve a counting uncertainty of 1%, it is necessary to measure ≈1 pL of $^{40}Ar^*$. For example, if one were to date a 100-Ma amphibole with a K concentration of 1000 ppm by laser microprobe, one would need to vapourize $\approx 10^6$ μm^3 (a 100-μm cube), while the scale at which the Malenco amphiboles are intergrown is much smaller (Fig. 5).

All five Ar isotopes were measured: ^{40}Ar, ^{39}Ar, ^{38}Ar, ^{37}Ar and ^{36}Ar. The age of a sample is calculated from the ratio of ^{40}Ar to ^{39}Ar. Because the irradiation of K, Cl and Ca produces ^{39}Ar, ^{38}Ar and ^{37}Ar respectively, the relative concentrations of these elements in the sample can be obtained from the Ar isotope data. As the amphibole overgrowth zones have a scale of several micrometres (Fig. 5), recoil of Ar isotopes during irradiation (Turner and Cadogan 1974; Villa 1997) is negligible. Therefore the $^{38}Ar/^{39}Ar$ and $^{37}Ar/^{39}Ar$ ratios of each heating step are a sufficiently good approximation of the Cl/K and Ca/K ratios of the phase that contributes most gas to that heating step.

It is well known (Lee et al. 1991; Wartho et al. 1991; Lee 1993) that amphibole releases its Ar in vacuo by a breakdown reaction. Lee et al. (1991) and Wartho et al. (1991) proposed that the ^{39}Ar release rate has three peaks as a function of temperature. Actually, Ca-derived ^{37}Ar is probably a better proxy for degassing of amphibole sensu stricto, as K-derived ^{39}Ar released below 1000°C could derive from minute K-rich impurity phases (Villa et al. 1996b, Fig. 2). The ^{37}Ar release in Wartho et al.'s (1991) and Lee et al.'s (1991) samples only shows two peaks which are identified as the breakdown by reaction to pyroxene + feldspar (B) and melting (M) respectively (Wartho et al. 1991). It is likely that Ar is expelled from the structure when a major rearrangement of structure-forming cations occurs. The data of Lee et al. (1991) and Wartho et al. (1991) imply that the most important cation rearrangement corresponds to reaction "B". In a mixture containing two or more amphiboles, and possibly other intergrown impurities, these additional reagents may enhance the overall reaction rate, and the temperature of the B degassing peak may be lowered. Texture and mineralogy may play an additional role; for example, they might be the cause of alternating degassing of the different components and contribute to the "crankshaft-style" release pattern in the high-temperature steps of some samples (S.P. Kelley, personal communication 2000).

Because of the compositional variability of amphiboles, their average ionic bond length/strength (Dahl 1996a) is different. The in vacuo breakdown rates are a function of binding energy and therefore a priori also expected to be different (cf. Dahl 1996b, p. 28; Villa et al. 1996a, Fig. 4c). Accordingly, the data from our laboratory in Fig. 3a shows that the peaks of the degassing rate of different amphiboles span a temperature interval of over 300 °C. This interval is wider than that reported by Lee (1993), as a larger range of amphibole compositions is considered here. The peak degassing temperature is a function of chemical composition and reflects Dahl's (1996a) predicted sequence. In most of these examples, the "B" peak is by far predominant and the "M" peak is small or non-existent. It is important to point out that all samples were analysed in the same furnace, so that effective crucible temperatures are not expected to be biased relative to each other.

To illustrate the possible role of zoned minerals on an age spectrum, a theoretical "stepwise heating experiment" has been modelled with a 200-Ma amphibole (am_1), rich in K and Ca, inter-/overgrown by a 100-Ma

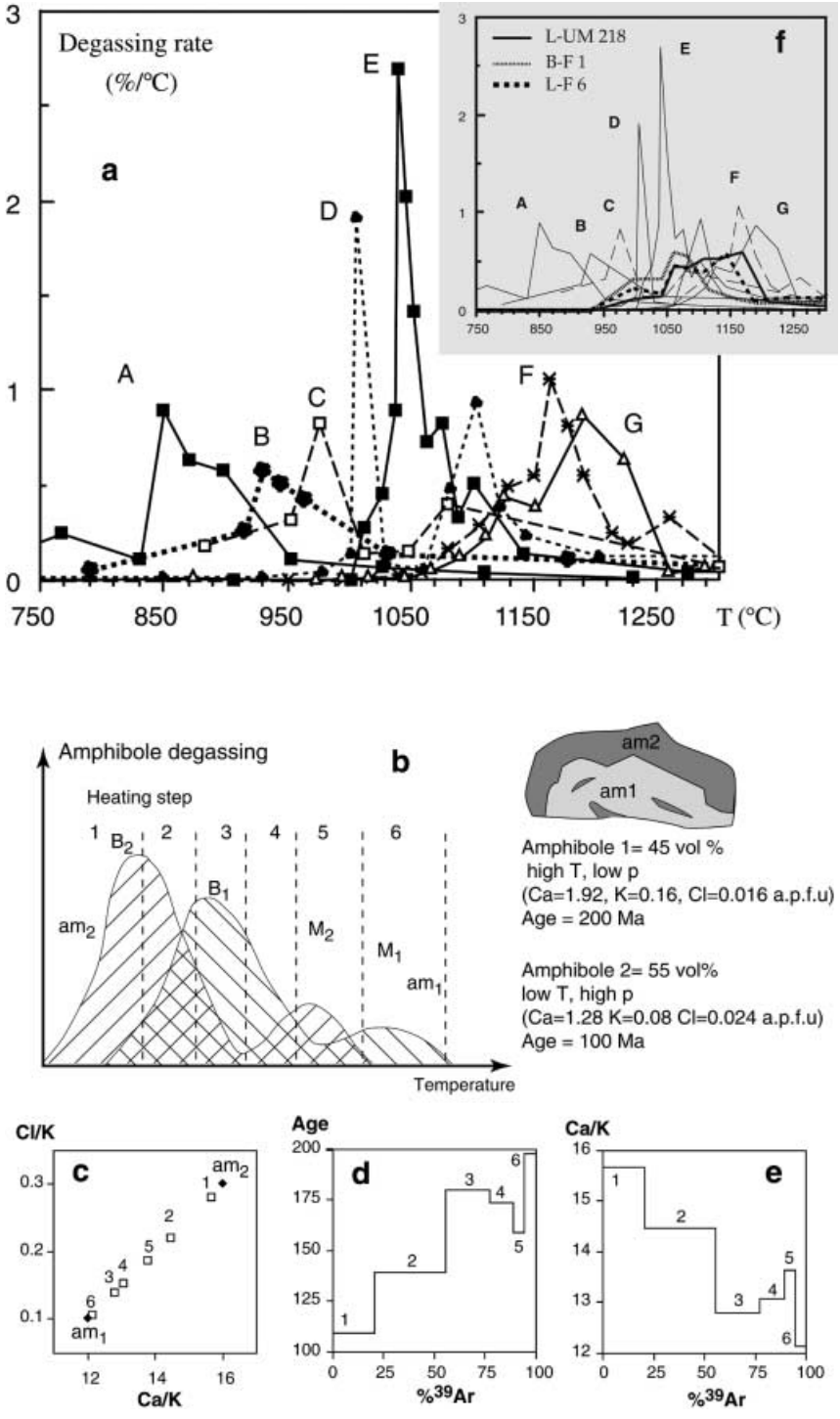

Fig. 3a Temperature dependence of degassing rate, i.e in vacuo breakdown temperature, for various amphibole compositions. *A* Riebeckite RT 48 (Handy et al. 1996); *B* Fe-richterite DG 102; *C* Fe-winchite DG 104 (*B* and *C* both Bortolotti et al. 1995); *D* actinolite AP 36 (Boriani and Villa 1997); *E* magnesiohastingsitic hornblende 93/533 (Kamber et al. 1995); *F* Mg-hornblende > tschermakite 95/625; *G* tschermakite > Mg-hornblende 95/655 (*F* and *G* both Belluso et al. 2000). **b** Schematic model of the degassing behaviour of a binary amphibole mixture. *B* breakdown of amphibole to pyroxene and plagioclase; *M* melting. **c** Chemical correlation diagram. In an ideal binary mixture the correlation is perfectly linear. **d** Age spectrum, **e** Ca/K spectrum, both showing irregularities. **f** Temperature dependence of degassing rate for the three samples from this study. The extended temperature interval over which degassing occurs, compared to the examples of Fig. 3a, argues for the presence of more than one amphibole composition (cf. Fig. 5)

amphibole (am_2) with lower K and Ca, and higher Cl contents (Fig. 3b). One amphibole (say am_2) degasses earlier than the other. The peaks of maximum outgassing, B_2 and M_2, are shown in Fig. 3b at lower temperatures than the corresponding peaks for am_1, B_1 and M_1. The gas released during each heating step is a variable mixture of gas from both amphiboles, and the resulting complexity of the age spectrum discourages a direct interpretation. However, by taking into account microchemical information we can resolve the mixture.

An interesting exception would occur if the two amphibole generations had exactly the same chemistry, because in that instance the peaks of maximum outgassing would perfectly overlap and the stepwise degassing would result in a constant Ar isotopic composition throughout the release. Due to the sensitivity of amphibole composition to the P–T conditions, formation of exactly isochemical amphiboles during two distinct metamorphic events seems rather unlikely.

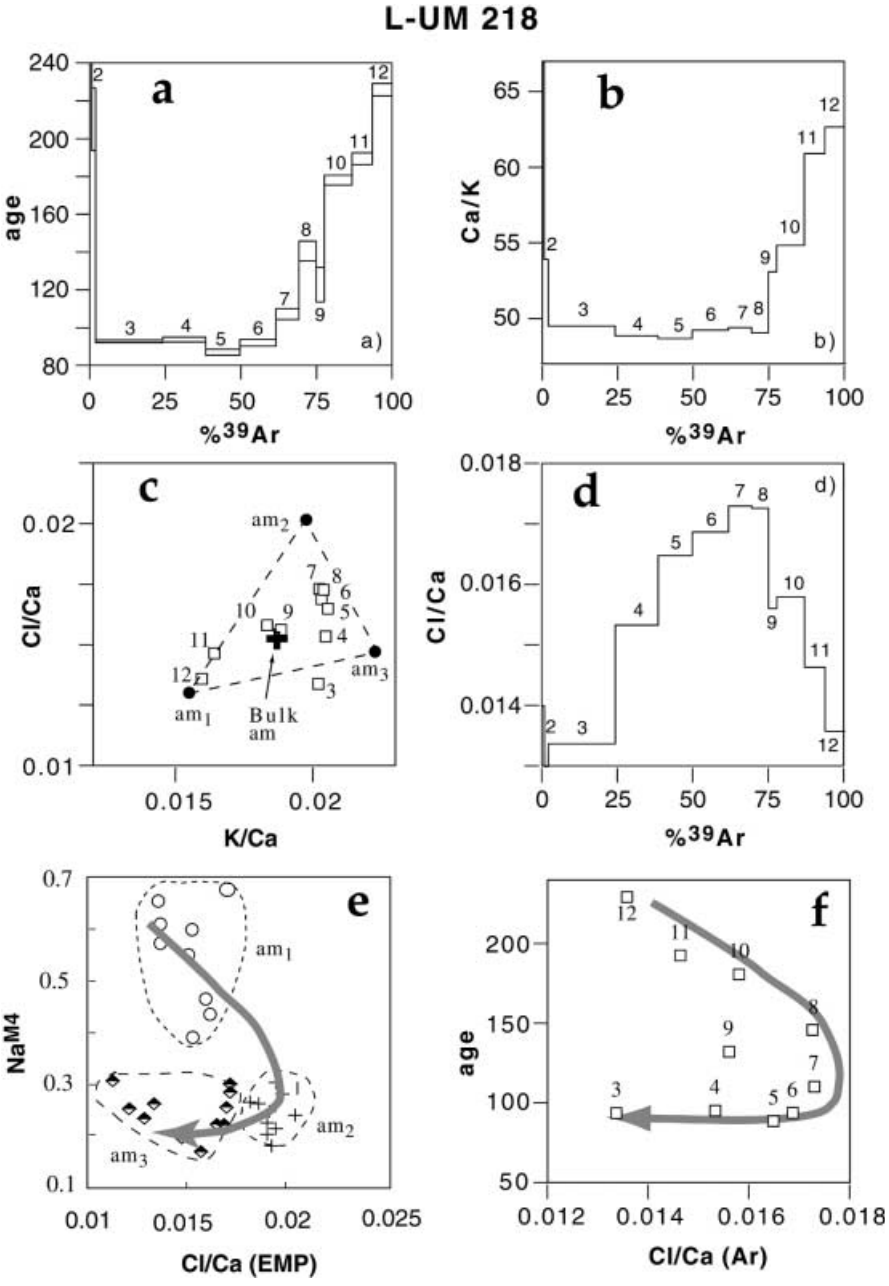

Fig. 4 Results for sample L-UM 218. **a** Age, **b** Ca/K and **d** Cl/Ca spectra. In the three-element correlation diagram **c** the data from stepwise heating (*open squares*; *numbers* refer to heating steps) are directly compared to microprobe analyses of average composition of amphiboles am_1, am_2 and am_3 (*filled circles*). The *minimum triangle* enclosing the Ar data coincides with the EMP data. Note that bulk extraction of Ca, K and Cl by the stepwise heating (*bold cross*; see Table 3) also lies within the triangle defined by the microprobe analyses. **e** Na^{M4} vs. chemical composition determined by EMP. The textural succession is indicated. **f** Age vs. chemical composition derived from Ar isotope ratios. The close relationship of the temporal evolution inferred from stepwise heating **f** with that derived from textures and microchemistry **e** permits a correlation between amphibole generation and age. Data points in **f** define a triangle, as in **c**, whose corners indicate ages of 225 Ma for am_1, 130–140 Ma for am_2 and ≤90 Ma for am_3

In the first heating step, am_2 is the dominant phase. Both the $^{37}Ar/^{39}Ar$ (Ca/K) ratio and the $^{38}Ar/^{39}Ar$ (Cl/K) ratio lie near the composition of pure am_2 (Fig. 3c); the Ar–Ar age is in the vicinity of the real crystallization age of am_2 (Fig. 3d). A higher proportion of am_1 than am_2 is outgassed in heating step three. This is mirrored in a significantly different chemical signature (Ca/K, Cl/K) as well as in an older age. The modelled age spectrum is rather irregular and does not evolve steadily from young to old ages. Equally erratic is the Ca/K spectrum (Fig. 3e). The whole spectrum is not at all a plateau. However, this does not imply that the spectrum is meaningless. The key to diagnosing the presence of a two-component mixture is shown in the chemical variation plot, Ca/K vs. Cl/K (Fig. 3c). In such a common-denominator three-isotope correlation diagram, it is simple to prove that ideal binary mixtures all lie on segments defined by the two components, and that *n*-component mixtures all lie within a convex *n*-polygon spanned by the *n* components (see also Belluso et al. 2000, p. 56; Villa 2000, Fig. 2). Figure 3c clearly indicates that a binary mixture of two amphiboles exists because all six steps lie on a line. The exact crystallization age of am_1 and am_2 cannot be read from the age spectrum (Fig. 3d). Nevertheless, a minimum age for the older amphibole is given by step 6, which corresponds to a chemical composition and age closest to the pure am_1, and a maximum age is obtained for am_2 in step 1.

While the sequence of breakdown reactions apparently complicates the age spectrum, it is still possible to

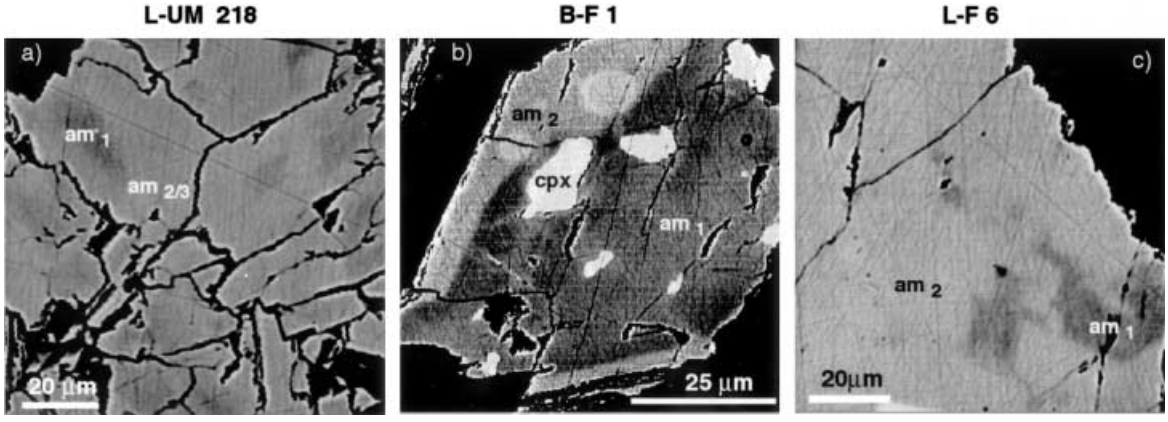

Fig. 5 Backscattered electron images of the mineral separates display the different generations of amphiboles. **a** Pre-Alpine amphiboles am_1 with high Na^{M4} values form rare cores within an am_2–am_3 matrix in sample L-UM 218. **b** Alpine pressure-dominated amphibole (am_1) with rare clinopyroxene inclusions (cpx) predominates in sample B-F 1. Am_1 is bordered by later amphibole am_2. **c** In sample L-F 6 am_1 occurs only as relics and the temperature-dominated amphibole am_2 predominates. *Scale bars* are 20, 25 and 20 µm respectively

exploit the wealth of information provided by the Ar isotopes produced from Ca, Cl and K (see Boriani and Villa 1997). As we have indicated in Fig. 3b, am_1 and am_2 are assumed to have Ca/K = 12 and 16, and Cl/K = 0.30 and 0.10 respectively. Then the Ca/K and Cl/K ratio of each step can be used to reconstruct the relative proportions of am_1 and am_2 in that step by mass balance (Fig. 3c). The sequence of the data points is not a monotonic one, but they define a linear correlation, as expected for binary mixing. The position of the two components is exactly specified in our forward model. In natural samples, however, it can only be inferred as upper/lower limit, unless independent chemical constraints (such as electron microprobe data) exist that fix the components precisely. If such microprobe data are available, it becomes straightforward to supplement the limited chemical information provided by the Ar isotopes (the Ca/Cl/K ratios for each heating step) with the full chemical composition that also includes elements (such as Si, Ti, Al, Na) that are not directly monitored by artificial Ar isotopes. This forms a link connecting the components identified from stepwise heating to the characteristic parameters describing petrogenesis. This aspect is illustrated below with microprobe data on natural samples.

While a linear array in the Ca/Cl/K diagram is the necessary consequence of a binary mixing, it could be argued that not all linear arrays are due to mixing. For instance, it could appear that in a chemically homogeneous amphibole with ''domain'' sizes smaller than the recoil length of ^{39}Ar, linear covariation could be an artefact due to mobility of the common denominator (i.e. removal or addition of ^{39}Ar by recoil). However, this is not a realistic explanation: firstly, because the magnitude of the required recoil redistribution needs to account for the whole range of Cl/K variations (often > 50%); secondly, because one of the numerators, ^{37}Ar, undergoes a greater recoil than ^{39}Ar; thirdly, because the same linear correlation is seen between other ratios, whose denominators are not as sensitive to recoil (e.g. Ca/Cl vs. Ar*/Cl).

The P–T evolution thus obtained can finally be combined with another common-denominator three-isotope correlation diagram such as Ca/K vs. Ar*/K. In this way it is possible to assign a K–Ar age to the components of the mixing. This assignment constrains the segment of the P–T–t evolution bounded between the earliest and the latest amphibole generation.

In summary, the procedure should include all of the following steps, in the correct order:

1. Plot Ar data in a common-denominator three-isotope correlation diagram.
2. Identify corners of *n*-polygon enclosing the data points.
3. Compare inferred chemical composition of these *n* corner-points with measured EMP data on Ca, K, Cl.
4. If they match, identify components as chemically (and mineralogically) distinct reservoirs.
5. By using a diagram correlating age with chemical composition, assign formation ages to each reservoir.

It is important to stress that these distinct Ar reservoirs are modelled by combining the Ar isotopic systematics with the microchemical data. The pure modelled compositions do not need to correspond to specific steps, and indeed may never be directly observed in the degassing of a polyphase aggregate due to possible partial overlap of their Ar releases. Only to the extent that clear and consistent corner-points of polygons are identified from the combination of Ar and EMP data is the present approach legitimate.

The use of Ar isotope systematics to extract chemical information has proved successful in the case of polymetamorphic amphiboles from the Limpopo Belt. In that instance, Belluso et al. (2000) obtained a close correspondence between the components derived from ^{39}Ar–^{40}Ar stepwise heating and those observed by analytical electron microscopy.

Table 3 Representative electron microprobe analyses of the pargasites. Cations are calculated using NAMP normalization. Mg# refers to total iron. Vector substitutions starting from tremolite are indicated

Sample	L-UM 218	L-UM 218	L-UM 218	B-F 1	B-F 1	B-F 1	L-F 6	L-F 6	L-F 6
Am type	am1	am2	am3	am1a	am1b	am2	am1	am2	am3
SiO_2	44.4	42.2	42.3	45.6	45.7	44.2	45.0	42.0	41.7
TiO_2	0.09	0.06	0.09	0.27	0.05	0.17	0.36	0.45	0.38
Cr_2O_3	0.62	0.09	n.a.	0.03	n.a.	n.a.	n.a.	n.a.	n.a.
Al_2O_3	17.5	17.5	15.9	14.7	18.1	16.7	12.2	14.7	14.7
Fe_2O_3	2.10	0.58	2.97	0.90	0.43	0.66	4.17	3.85	2.90
FeO	5.48	7.40	6.26	5.36	4.44	4.89	11.8	13.5	13.4
MnO	0.11	0.18	0.18	0.13	0.07	0.13	0.31	0.28	0.25
MgO	13.5	13.9	14.7	15.5	15.1	16.2	10.7	9.27	9.70
NiO	0.31	< 0.04	n.a.	< 0.04	n.a.	n.a.	n.a.	n.a.	n.a.
CaO	9.71	11.8	11.7	10.3	9.14	11.9	9.05	10.0	10.4
Na_2O	4.77	4.10	4.05	4.53	5.57	4.13	4.49	4.15	4.12
K_2O	0.14	0.23	0.22	0.40	0.37	0.44	0.39	0.64	0.54
Cl	0.07	0.18	0.11	< 0.02	< 0.02	< 0.02	< 0.02	< 0.02	< 0.02
H_2O	2.11	2.04	2.09	2.11	2.16	2.14	2.04	2.03	2.01
Σ	100.9	100.2	101.7	99.9	101.1	101.6	100.4	101.0	100.1
Si	6.26	6.07	6.14	6.47	6.35	6.19	6.59	6.21	6.20
Ti	0.01	0.01	0.01	0.03	0.01	0.02	0.04	0.05	0.04
Cr	0.07	0.01	–	0.00	–	–	–	–	
Al	2.90	2.96	2.66	2.46	2.96	2.75	2.10	2.56	2.59
Fe^3	0.22	0.06	0.32	0.10	0.05	0.70	0.46	0.43	0.33
Fe^2	0.65	0.89	0.75	0.64	0.52	0.57	1.45	1.67	1.66
Mn	0.01	0.02	0.03	0.02	0.01	0.02	0.04	0.04	0.03
Mg	2.84	2.98	3.09	3.28	3.11	3.39	2.33	2.04	2.15
Ni	0.04	0.00	–	0.00	–	–	–	–	
Ca	1.47	1.82	1.78	1.56	1.36	1.78	1.42	1.59	1.66
Na	1.30	1.14	1.11	1.25	1.50	1.12	1.28	1.19	1.19
K	0.03	0.04	0.04	0.07	0.07	0.08	0.07	0.12	0.10
Cl	0.02	0.04	0.03	0.00	0.00	0.00	0.00	0.00	0.00
H	1.98	1.96	1.97	2.00	2.00	2.00	2.00	2.00	2.00
Mg#	0.77	0.76	0.74	0.82	0.85	0.84	0.55	0.49	0.52
Tschermak	1.47	1.11	1.14	1.09	1.37	1.05	1.22	1.30	1.20
Edenit	0.80	1.00	0.94	0.88	0.92	0.98	0.77	0.90	0.95
Na(M4)	0.53	0.18	0.22	0.44	0.64	0.22	0.58	0.41	0.34

Results and discussion

Pre-Alpine relics: amphibolite pyroxenite L-UM 218

Microchemistry

Microprobe analyses reveal that three different amphibole types have been preserved (Fig. 4 and Table 3). BSE images (Fig. 5a) show a distinct zonation between am_1 and am_2; am_2 predominates over am_1. Am_2 and am_3 cannot be distinguished by BSE images; however, am_3 which rims am_2 has a lower Cl/Ca ratio. The three amphibole generations have different chemical compositions (Table 3). Am_1 has higher Na^{M4} and lower Cl contents and a higher Ca/K ratio with respect to am_2. Am_2 and am_3 can be distinguished by their chlorine contents, 1,800 and 1,100 ppm respectively.

^{39}Ar–^{40}Ar dating

The age spectrum is shown in Fig. 4a. The first two heating steps, containing a very small proportion of the total Ar, feature Ca/K and Cl/K ratios markedly different from the rest of the heating steps (Table 2). The identification of these steps as degassing of minor alteration phases follows Villa et al. (1996b), who related the anomalous Ca/Cl/K ratios to the TEM observation of secondary minerals. Amphibole sensu stricto is only degassed from step 3 onwards. In the first section (75% of the release, between steps 3 and 8), the Ca/K ratio remains constant (Fig. 4b), but the Cl/Ca ratio steadily increases (Fig. 4d). From steps 8 to 12, Cl/Ca reverses its trend and decreases, while Ca/K monotonically increases.

The behaviour of the step ages also shows a rational pattern. Heating steps 7 and 8 exhibit the highest apparent ages of the first section. This indicates that (1) an Ar reservoir exists with a high Cl/Ca ratio and comparatively high ages and (2) the apparent "plateau" spanning steps 3 to 6 is an artefact without geological significance (cf. Villa et al. 1997, Fig. 2) and represents a mixing between younger (Alpine) and older (pre-Alpine) ages.

The step heating points are compared with the microprobe data in Fig. 4c. It is clear that the two data-sets are closely related. In this correlation diagram, the linear

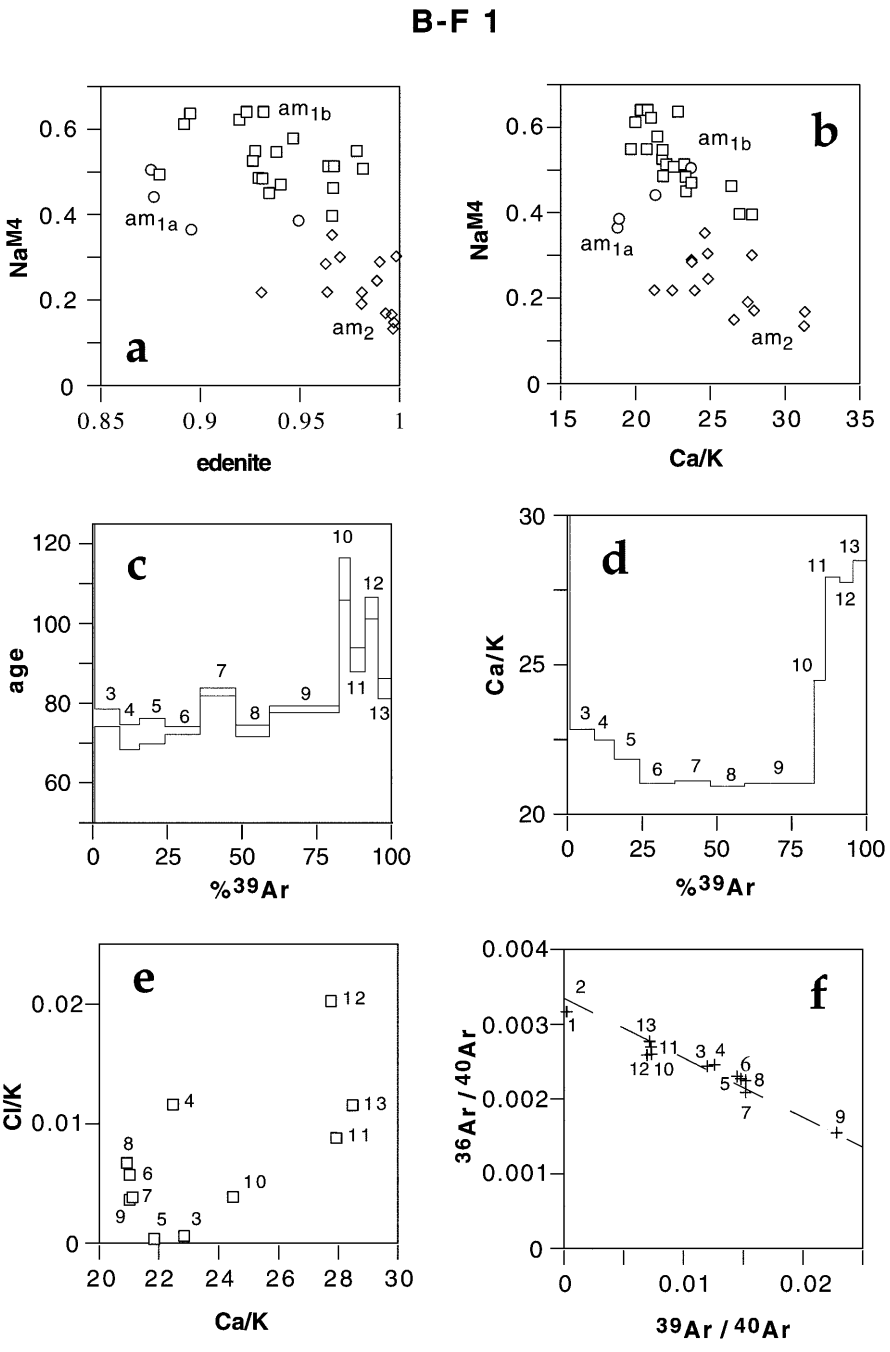

Fig. 6 Results for sample B-F 1. **a**, **b** Composition of different amphibole generations, **c** age spectrum, **d** Ca/K spectrum, **e** three-element correlation diagram from stepwise heating. Numbers refer to heating steps. In the isochron plot, **f**, the regression line has an excessively high scatter (MSWD = 17), i.e. the sample does not meet the requirement of a monogenetic, isochronous origin

trends of steps 3–8 and 8–12 are interpreted as dominantly binary mixtures between reservoirs am_2–am_3 and am_1–am_2 respectively. The similarity between the Ar stepwise release data and the microchemistry is readily understood as differential breakdown of different amphiboles.

The degassing rate of L-UM 218 is shown in Fig. 3f. In contrast to the narrow peaks of Fig. 3a, this sample releases its Ar over a broad temperature interval. This is an additional argument for the presence of more than one amphibole composition, in addition to the electron microprobe observations and Ar correlation diagrams.

Interpretation

Textural relationships unambiguously indicate that am_3 is younger than am_2 and am_2 is younger than am_1. This provides support for our isotopic identification of three chemically and temporally distinct amphibole generations. The correlation plot in Fig. 4f (age vs. Cl/Ca) allows us to assign each of the three inferred amphibole components a K–Ar apparent age. However, estimating components is always underconstrained, and it is clear that the age assignments are only maximum (or minimum) values.

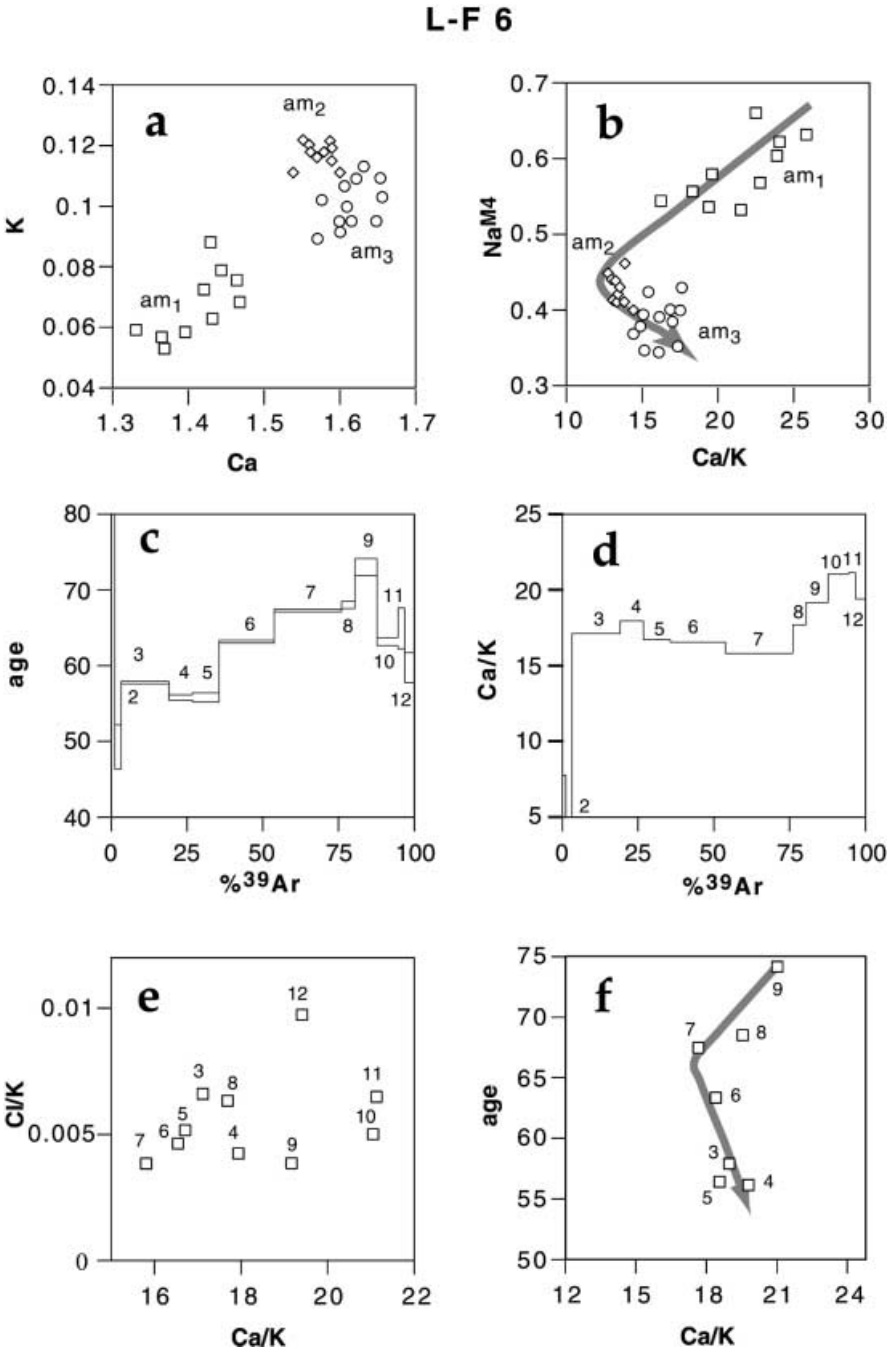

Fig. 7 Results for sample L-F 6. **a**, **b** Composition of different amphibole generations, **c** age spectrum, **d** Ca/K spectrum, **e** three-element correlation diagram and **f** age vs. chemistry plot resulting from stepwise heating. *Numbers* refer to heating steps. Note the close relationship of temporal evolution from stepwise heating **f** and from textures and microchemistry **b**

The correlation between chemical element ratios and age as we propose it in Fig. 4e, f would assign a maximum age ≤90 Ma for am_3. The chemical signature of the high-temperature steps (10–12), on the other hand, gradually approaches the measured chemical composition of am_1 (Fig. 4c). Steps 11 and 12 have the highest Ca/K ratios and lie on the tieline between am_1 and am_2 in Fig. 4c, i.e. they result from simple binary mixing. An age of 225 Ma for the pure am_1 reservoir is calculated as the asymptote of the final heating steps in a correlation diagram of Cl/Ca vs. age (Fig. 4f). Two factors limit the precision of the am_1 age estimate: (1) the rather low K and Cl concentrations which result in a significant scatter of K/Ca and Cl/Ca ratios in the EMP analyses, and thus make the chemical fingerprint of the component imprecise; and (2) the possible presence of excess Ar. It is necessary to clearly distinguish between "excess Ar" and "inherited Ar" (we follow the strict definition by Lanphere and Dalrymple 1976). In our samples, there is no evidence that step ages are any older than that which can be accounted for by inheritance only. We therefore maintain that excess Ar was not an important factor in the Malenco amphiboles.

The formation age of am_2 is more difficult to estimate, as all intermediate steps contain some Ar from

am_1 and am_3. In the chemical correlation diagram (Fig 4c), the vertex corresponding to am_2 is inferred to have Cl/Ca > 0.175, K/Ca = 0.02; in the age-Cl/Ca diagram (Fig. 4f) this vertex has an age of 130–140 Ma.

An additional by-product of our approach is insight into the petrologic evolution. By determining a parameter such as Na on the M4 site on the same amphibole for which we have estimated an age, we are able to estimate the relative formation pressure corresponding to the K–Ar age of individual amphibole generations obtained from Fig. 4c, f.

In terms of metamorphic conditions, the texturally oldest amphibole (am_1) exhibits the highest Na^{M4}, indicating formation under relatively high pressures. It has an apparent age of ≈225 Ma. If this age is interpreted as true, then the evolution of L-UM 218 acquires the following meaning. Am_1 formed at relatively high pressures at ≈225 Ma during an initial stage of rifting. A second pre-Alpine amphibole (am_2) crystallized under relatively low pressure as indicated by low Na^{M4}. It shows elevated Cl/Ca ratios (and high Cl and K contents) and has an age around 130–140 Ma. Am_2 and am_3 are not distinguishable on the basis of their Na^{M4} content, but of their Cl/Ca ratio. Modelling the third component (am_3) from Fig. 4c, f gives an apparent age of 87 to 93 Ma, approaching the age of early Alpine metamorphism. The Alpine evolution will be addressed in the following paragraph.

Alpine amphiboles

Two Alpine pargasites were analysed from pargasite-bearing gabbro dyke B-F 1 and pargasitic blackwall L-F 6. Petrographic observations suggest a different preservation of pre-Alpine relics: in B-F 1 the gabbroic texture is still clearly recognized, while in L-F 6 recrystallization was pervasive (Fig. 2b).

Pargasite-bearing gabbro B-F 1

Microchemistry

The BSE images of the amphibole separate (Fig. 5b) show a strong zonation with relict clinopyroxene, idiomorphic pargasites (am_1) and a later rim (am_2). Am_1 is more abundant than am_2. Within am_1 an older amphibole generation am_{1a} could be detected that displays only a weak BSE contrast to the more abundant amphibole am_{1b}. The amphiboles have different chemical characteristics. Am_{1b} displays the highest Na^{M4} content of 0.66 and a constant Ca/K ratio (Fig. 6a, b). Unfortunately, the Cl concentration in these amphiboles is mostly below the detection limit of 0.01 wt% and therefore makes meaningful Cl/K microprobe measurements impossible. The Ca/K ratio of am_2 overlaps the range of am_{1b} but partly displays higher values. Am_2 is characterized by significantly lower Na^{M4} (0.21) and slightly higher edenite content than am_{1b}. Am_{1a} can be distinguished from am_{1b} by slightly lower edenite and Na^{M4} contents.

The textural and chemical information permits correlation of amphibole growth to the Alpine P–T path (Fig. 2a). Am_{1b} recrystallized during the recorded peak pressure. Am_2 may be correlated to peak temperature that occurred at significantly lower pressure. Am_{1a} most probably formed during prograde metamorphism near peak pressure conditions.

^{39}Ar–^{40}Ar dating

The age and Ca/K spectra (Fig. 6c, d) show less pronounced variations than those of L-UM 218. In particular, the Ca/K ratio (Fig. 6d) only varies between 21 and 23 over 80% of the release.

In the chemical correlation plot (Fig. 6e) steps 5–9 are aligned along a well-defined line with a negative slope. This line, and the anticorrelation of Cl with Ar* (Table 2), both mean that the mineralogical difference seen by EMP is reflected in the Ar systematics, and we attribute the higher ages to the Cl-poor component am_1, and the lower ages to am_2. Steps 10–13 show the highest Ca/K ratios and the highest age. The higher ages might be due to excess argon (either in amphibole or in pyroxene); however, there are two arguments that step ages around 100–110 Ma are meaningful.

1. The chemical signature – especially of step 12, which yields the highest age – is different from the composition of the other amphiboles indicating that an additional component has to be considered. This component is significantly richer in Cl. Cl is unlikely to be contained in saline fluid inclusions, as absorbed electron imaging shows that Cl is rather homogeneously distributed within amphibole. Apatite inclusions have very high Cl/Ca ratios (Belluso et al. 2000), different from that of steps 10–13. Pyroxene has no Cl substitution in its stoichiometry. We therefore believe it is more likely that this component is correlated to the pre-Alpine, high-Cl amphiboles detected in sample L-UM 218.

2. Although our 26 electron microprobe point analyses on the mineral separate do not unambiguously discriminate am_1 from am_0, textural evidence for a pre-Alpine amphibole generation is provided by pargasite inclusions in pre-Alpine grossular (Fig. 2b). While it is impossible to decipher the presence or absence of excess Ar if only sample B-F 1 is taken into account, we believe that the geological context (a regional Jurassic amphibole formation) and the comparison with related sample L-UM 218 argue against excess Ar.

Finally, an isochron plot is shown in Fig. 6f. As can be seen, the data points plot near, but not on, a 72 Ma regression line. While this age may seem a legitimate average, it is not, because of two reasons.

1. A real isochron that corresponds to a geologically meaningful age is a two-component mixture between

one single trapped Ar and one single radiogenic component. In Fig. 6f, the dispersion of the data about the 72 Ma regression line by far exceeds statistical fluctuations, as MSWD = 17. By definition, the points must not be regarded as defining a two-component isochron; at least a third, different Ar reservoir is involved.

2. This additional reservoir is suggested by the other isotope correlation plots discussed above. Since this sample consists of at least two intergrown amphiboles, it is clearly arbitrary to pretend that they have a single radiogenic component (i.e. the same age) and that they trapped the same initial Ar.

Interpretation

The interpretation of the age spectrum must take into account mineralogy. Since the Ca/K ratio measured by EMP is very similar in amphiboles 1 and 2, and the Cl concentrations are below the detection limit of the electron microprobe, it is not possible to estimate components by mass balance as was done for L-UM 218. However, textural relationships and geological constraints may help to correlate heating steps with amphibole generations. BSE images indicate that am_1 and am_2 are the most abundant amphiboles in the separate. Therefore they should be related to the heating steps 6–9, which contain about 60% of the total ^{39}Ar. These four steps have a very similar, low Ca/K ratio, in agreement with the compositions determined by EMP. Amongst them, two steps show lower Cl/K, slightly higher Ca/K ratios and higher ages (steps 7 and 9), and are tentatively equated to am_1. Steps with lower Ca/K, higher Cl/K and lower ages (6 and 8) are assigned to am_2. We note that this attribution is not only based on small age differences (in which case it would be underconstrained), but rather on the chemical correlation.

The age of the pure, Cl-poor component am_1 is inferred to be >83 Ma. In Fig. 7e, the position of the am_1 component is most closely approximated by step 7 (with a step age of 83 Ma; Fig. 7f), which nevertheless still contains Ar from the younger am_2 rims. In turn, the age of component am_2 is a function of both the fractional contribution of am_1 to steps 6 and 8, and of the latter's true age; in any case, am_2 has to be no older than the age of step 6 or 8, i.e. 73 Ma. From step 10 onwards, the Ca/K rises sharply. We interpret this as one (or more) pre-Alpine relict amphibole am_0, and the highest observed step age of 110 Ma as its minimum age. This age is away from the true formation age because the mass fraction of this amphibole generation is very small. If these pre-Apline relics are too small for unambiguous EMP detection (<1 μm) then Ar recoil during irradiation becomes significant. In this case, differential recoil redistribution of ^{37}Ar, ^{38}Ar and ^{39}Ar might explain some irregularities of the last four steps.

On the other hand, a constraint on the age of am_1 is provided by step 11: if this step is interpreted to reflect a mixture between am_0 and am_1, it follows that pure am_1 must be younger than the step age, 91 Ma. In the high-Ca/K steps the modal proportion of cpx is low, as indicated by the comparatively high Cl/Ca ratio.

The chemical element ratios permit us to make a connection between age and petrologic indicators, as seen above. Am_1, with its high Na^{M4}, corresponds to a pressure-dominated metamorphism, for which we estimate an age between 83 and 91 Ma. Am_1 is the predominant amphibole in sample B-F 1. Am_2 rims document a pressure decrease and possibly a temperature increase, as K increases; we assign them an age <73 Ma.

Pargasitic blackwall L-F 6

Microchemistry

The BSE images of grain mounts display two distinct amphibole generations. Am_1 occurs as irregular small cores within a younger am_2–am_3 mixture that predominates (Fig. 5c). Chemical analyses of the separated amphiboles provide evidence for three distinct amphibole compositions (Fig. 7a, b). Am_1 contains little Ca and correspondingly high Na^{M4}, similar to am_1 in sample B-F 1. Am_2 has significantly higher Ca and K contents. The Ca content of am_3 is again higher, whereas the K trend is reversed. This leads to a characteristic Ca/K ratio for each of these three amphibole types.

From texture and chemical composition the amphibole generations can be correlated to the Alpine P–T evolution (Fig. 2a). The relict am_1 has the highest Na^{M4} contents and is texturally oldest. It crystallized at highest pressure conditions. From am_1 to am_2 to am_3 the Na^{M4} content decreases. We interpret this, together with the textural relation, as indication for a pressure decrease illustrated in the P–T path (Fig. 2a). The Na^{M4} content can thus be used as a relative time marker. Am_2 displays a significantly higher K and edenite content than am_1 and is correlated to peak temperature conditions. Am_3 is interpreted to have formed under retrograde conditions. We note that, unlike B-F 1 (where the oldest amphibole generation had a chemical evolution that does not lead to the am_2 generation), in L-F 6 am_1 and am_2 appear to grade into each other (Fig. 7b).

^{39}Ar–^{40}Ar dating

The Ca/K ratio and the age spectrum both show a complex behaviour (Fig. 7c, d). Steps 1 and 2 were identified as alteration products on account of their Cl/Ca/K signature (Table 2), as discussed for L-UM 218. In the three-element correlation diagram (Fig. 7e), the heating steps 3, 5, 6 and 7 are aligned along a first mixing line and the steps 7, 9 and 10 form a second mixing line. This suggests that three amphibole generations are involved in the degassing, which is in agree-

ment with the microchemical investigation (Fig. 7a). In the age vs. Ca/K diagram (Fig. 7f) we observe a systematic evolution, with the Ca/K ratio first decreasing up to step 7 and later increasing again.

Interpretation

The Ca/K ratio determined by microchemistry (Fig. 7b) and in the Ar–Ar analyses (Fig. 7f) permits a correlation of the heating steps with the different amphibole generations. The predominant amphibole am_2 is best represented by heating step 7 which displays the lowest Ca/K ratio. Accordingly, steps 3–6 are interpreted to result from degassing of a mixture between am_2 and am_3. Because of its small mass fraction, am_1 gas is never completely pure in any step, and therefore the Ca/K ratio never exceeds 21 in the Ar data while it reaches 26 in the EMP data. The steps with highest ages, 7–9, originate from a mixture between am_1 and am_2. The age of am_1 is thus ≥73 Ma. This minimum age is compatible with the 83–91 Ma inferred from sample B-F 1. This less tight constraint is easily explained by the observation that in sample B-F 1 the most abundant amphibole is am_1 whereas in L-F 6 it is the younger one, am_2. The age of am_2 can be estimated from steps 4–7, which account for ≈60% of the total ^{39}Ar release. The mixing indicates a maximum age of 55 Ma for am_3 and a minimum age of 67 Ma for am_2. From B-F 1 we have derived a maximum age for am_2 of ≈73 Ma. This means that the second phase of amphibole growth occurred between 67 and 73 Ma, at the temperature peak of the Alpine cycle.

The role of diffusion

The Malenco amphiboles provide the opportunity to compare laboratory-based and field-based estimates for the diffusion of Ar. As was mentioned earlier, the temperature reached by Malenco rocks during Alpine metamorphism was about 450 °C.

Of special interest is the laboratory determination of the Ar diffusivity in hornblende. The laboratory phenomena have been reviewed and discussed by Villa et al. (1996b) and it is now clear that several artefacts had plagued the earlier determinations (Villa et al. 1996b, pp. 78–79). As shown by these authors, the true diffusivity is at least one order of magnitude lower than that used by McDougall and Harrison (1988). With the new diffusivity data it is straightforward to calculate that for an ambient T = 450 °C and a heating duration of 20 Ma (Fig. 8) the mean diffusion length of Ar was 2.5 μm, insufficient to significantly affect the Ar* budget of our samples.

Do the Malenco amphiboles conform to this expectation, or do they show a reduced retention of radiogenic Ar*? Pre-Alpine relics that are petrographically visible appear to have preserved a significant proportion of their Ar*. This observation confirms that diffusive loss of Ar has been negligible during the Alpine P–T loop. The pre-Alpine amphiboles sensu stricto, am_1 and am_2 of sample L-UM 218 and am_0 of sample B-F 6, retained a well-distinguishable Ar signature. They were largely unaffected by the formation (by local reaction leading to recrystallization) of am_3 and am_1 respectively, in the Cretaceous.

The Ar retention of our diachronically grown, heterochemical amphibole generations provides support for the conjecture that petrographic relics always carry

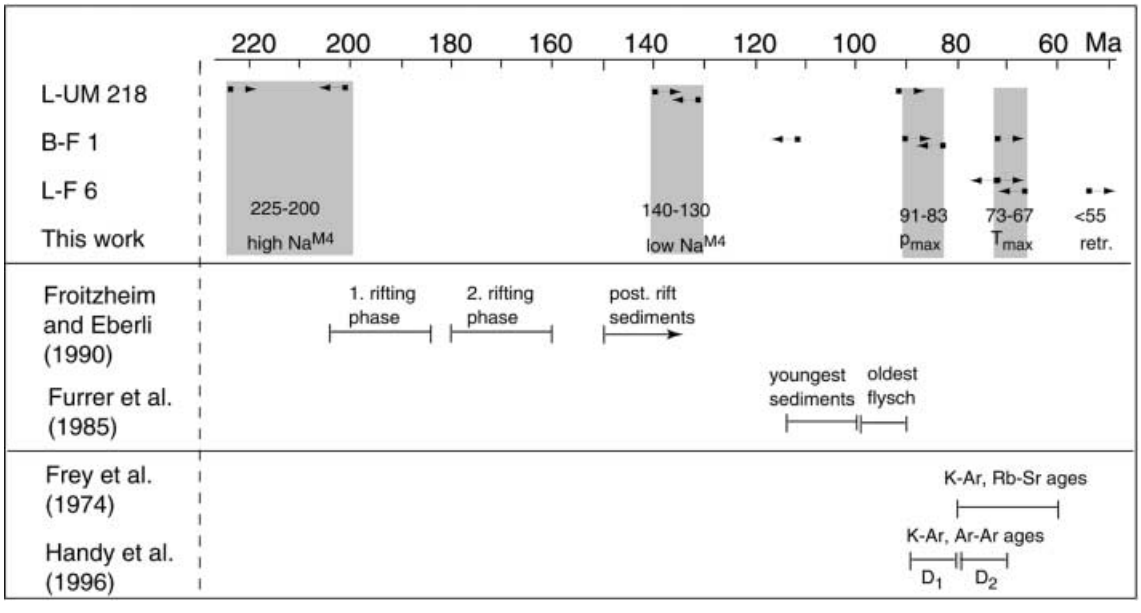

Fig. 8 Summary of age information of the three samples analysed. *Arrows* indicate obtained minimum/maximum ages, the *grey field* corresponds to the probable time span of amphibole formation. The data are compared to age constraints from Austroalpine sediments (Furrer et al. 1985; Froitzheim and Eberli 1990) and to previous radiometric age determinations in the Penninic–Austroalpine boundary region (Frey et al. 1974; Handy et al. 1996)

isotopic inheritance (Villa 1998, p. 44) because trace elements, including radiogenic Ar, cannot diffuse faster than the structure-forming major cations.

Internal consistency

The three discussed age spectra of polymetamorphic amphiboles are very complex and thus might have been considered worthless. Nevertheless, we have applied an approach that relates the isotopic data to independent, external support, such as textural and microchemical information. We assigned ages to all amphibole generations; these ages are not very precise and are restricted to minimum and maximum estimates. Only the combination of three samples having different Alpine overprint permits us to constrain the age of the four metamorphic phases (Fig. 8). It is clear that with internal criteria alone it is impossible to decipher these spectra.

How well founded is the interpretation of internally discordant age spectra as reflecting mixtures of different mineral generations? BSE images of the separates provide relative ages of amphibole formation which agree with the age sequence deduced from the Ar–Ar ages. The known chemical evolution of amphiboles in the investigated area give further age constraints: it is known that the pre-Alpine amphiboles evolve from high Na^{M4} and intermediate Cl concentrations to low Na^{M4} and high Cl (Müntener 1997). This evolution is again in agreement with our interpretation of the spectra. The BSE images further show which amphibole generation is dominant in a sample. Pre-Alpine amphiboles are well preserved in L-UM 218, resulting in a spectrum with half of the step ages exceeding 110 Ma. Sample B-F 1 contains mostly amphiboles of the first Alpine generation, whereas the second Alpine generation predominates in L-F 6. Accordingly, the prevalent ages are older in B-F 1 than in L-F 6. Hence, the tightest bracket for an amphibole generation is always given by the sample in which this generation is petrographically predominant; the other samples can provide a consistency control on this age bracket.

The P–T–t evolution

Combining the data from all three samples, we have estimated the age ranges for the formation of the different amphibole generations shown in Fig. 8. It would appear that the uncertainty ranges for a single amphibole generation are quite large; however, the novelty of our approach is that estimates can be made at all on polymetamorphic rocks, in a way that satisfies the desire to take into account petrological information such as pressure, temperature and fluid composition. Furthermore, even if the ages that we infer for our samples may appear at first sight ambiguous and imprecise when one limits oneself to individual samples, it is the context of all samples together that should be considered.

Our data suggest that the first pre-Alpine amphibole generation formed around 225 Ma at lower crustal levels as documented by high Na^{M4} contents. The second pre-Alpine amphibole generation formed around 130–140 Ma and displays an increase in Cl content and a decrease in Na^{M4} (see Fig. 4e, f) consistent with possible interaction with seawater-derived fluids. Hydration, decompression and exhumation to the seafloor are likely to be associated with Jurassic rifting (Fig. 9).

In the investigated area, the earliest Alpine metamorphism is pressure-dominated and minerals grew synkinematically with respect to the first deformation D_1. This deformation is related to the stacking of nappes. The Na^{M4} values of our samples are consistent with 0.5–0.6 GPa determined in mafic rocks, with temperatures around 400–450 °C (Bissig and Hermann 1999). We attributed an age of 83–91 Ma to this amphibole generation.

The synkinematic metamorphism at peak pressures is followed by a thermal peak. Increasing temperatures ($T \approx 450$ °C; Fig. 9) are documented in the Malenco unit by chemical zoning of garnets in mafic rocks (Hermann 1997). As seen above, in this temperature range diffusion of Ar out of amphibole is negligible, and the ages can be safely interpreted as formation ages. A second generation of amphiboles has formation ages of ≈67–73 Ma. Amphibole composition indicates a significant decrease in pressure. This is in good agreement with structural observations in the overlying Austroalpine units. There, the D_2 deformation is interpreted as extensional, leading to the collapse of the nappe pile accompanied by a pressure decrease (Hermann and Müntener 1992; Liniger 1992; Spillmann 1993). As second-generation amphibole growth

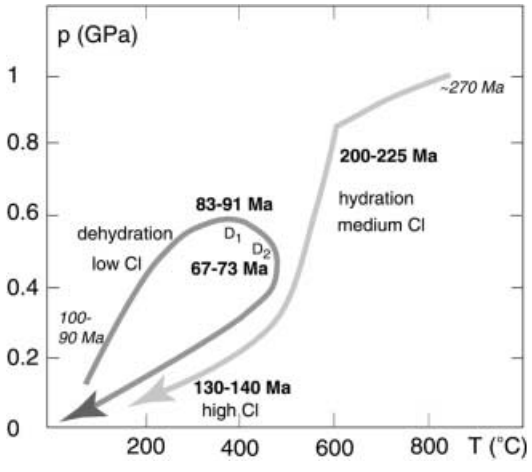

Fig. 9 Compiled P–T–t–fluid path. The ages obtained by this study are indicated in *bold*. Pre-Alpine retrograde hydration is characterized by an increase of Cl in the fluid. By contrast during Alpine dehydration the Cl content of the fluid is very low. Independent age constraints are shown in *italics* [U–Pb on zircons for the Braccia gabbro intrusion (Hansmann et al. 1996); age of post-rift sediments (Froitzheim and Eberli 1990) and of first flysches (Bernoulli and Winkler 1990)]

occurred at 67–73 Ma and contemporaneous or later than D_2 extension (Fig. 9), both nappe formation and later extension are of Cretaceous age (see also Handy et al. 1996).

A still later phase of amphibole growth, younger than 54 Ma, is documented in sample L-F 6. New growth of pargasites is documented in axial plane foliations of later backfolding events and in shear bands cutting the pargasite foliation (Fig. 2b). The latter have a low Na^{M4} content, indicating a further pressure decrease relative to the second generation (see Hermann 1997).

External control

What are the independent, non-isotopic constraints which can support or contradict our reconstruction of the Jurassic–Cretaceous P–T evolution?

The formation of the first pre-Alpine amphibole generation is attributed to hydration at the onset of Jurassic rifting (Müntener et al. 2000). The second pre-Alpine generation was produced by hydration and exposure to saline fluids near the seafloor. The inferred ages are in good agreement with the sedimentary record of the Austroalpine continental margin. The first amphibole generation is inferred to have formed during the first rifting phase of Froitzheim and Eberli (1990; Fig. 8). The second generation, formed close to the ocean floor, post-dates rifting (Fig. 8). It is noteworthy that oceanic crust formation in the nearby Platta unit has been dated at 161 ± 1 Ma (Desmurs et al. 1999) on single zircon grains from oceanic gabbros.

The age of Alpine metamorphism in the Malenco area is also constrained by the sedimentary record. The youngest sediments incorporated in the nappe pile are Turonian (Finger 1978; Caron et al. 1982). Consequently, the metamorphism must be post-Turonian, i.e. younger than ≈90 Ma according to the time-scale of Haq and Eysinga (1987). On the other hand, Cretaceous flysch sediments (Bernoulli and Winkler 1990) indicate that relief caused by convergence was well developed before ≈90 Ma. Thus, the sedimentary record requires active tectonics in Turonian times.

The ^{39}Ar–^{40}Ar ages presented here can be compared with data reported from the overlying Margna nappe (Fig. 1). Age determinations of the Alpine metamorphism on white mica (Rb–Sr) and on biotite (K–Ar, Rb–Sr) given in Frey et al. (1974) scatter between 60 and 80 Ma and are generally in agreement with the data presented here (Fig. 8). However, one problem with these data is that the bulk extraction techniques (K–Ar, Rb–Sr) lack the resolution of the ^{39}Ar–^{40}Ar stepwise heating method and most probably the ages reported by the authors represent mixing ages between minerals of the two generations discussed here. The Cretaceous, P-dominated amphibole growth overlaps with the timing of peak pressure in the Austroalpine high-P belt between Saualpe and Ötztal (Thöni and Jagoutz 1993).

The ages of the Alpine metamorphism presented here agree with data from the Penninic–Austroalpine boundary further to the north reported by Handy et al. (1996). These authors report 80–88 Ma for the pressure-dominated first metamorphism on the basis of D_1 synkinematic phengites dated with the K–Ar method (Fig. 8). D_2 synkinematic amphiboles (^{39}Ar–^{40}Ar) and phengites (K–Ar) have crystallization ages of 69–80 Ma. This is comparable to the thermal peak of 67–73 Ma which follows the D_2 extension (Fig. 9).

The proposed P–T–t evolution for the Malenco unit is thus in agreement with sedimentological and isotopic data of adjacent geological units. The Late Cretaceous ages for Alpine metamorphism further strongly support an origin of the Malenco unit from the Adriatic continental margin.

Conclusions

1. Amphiboles in the polymetamorphic Malenco unit consist of several generations that crystallized under different P–T conditions. The isotopic record of each generation is largely unaffected by the crystallization of texturally younger amphiboles.
2. Chronological information can be extracted from irregularly discordant ^{39}Ar–^{40}Ar age spectra; ''plateaus'' are not a prerequisite for successful dating.
3. The in vacuo breakdown properties of a mineral are determined by its interatomic bond length/strengths. The release of Ar from a mineral mixture will therefore have a different temperature dependence for each mineral. The Ar isotope ratios enable identification of heterogeneous components (i.e. reservoirs) in a ^{39}Ar–^{40}Ar stepwise heating experiment.
4. Mixing components inferred from the Ar isotope correlation diagrams are indistinguishable from the compositions determined by electron microprobe on texturally distinct amphibole generations. The identity of the chemical signatures obtained in two independent ways gives confidence that the systematic behaviour of mixtures is correctly understood.
5. The treatment of amphibole generations in terms of diagrams correlating ages with chemical composition provides a link between compositional parameters of one particular amphibole generation, such as Na^{M4}, with the K–Ar age of that same generation.
6. Relating ^{39}Ar–^{40}Ar data to petrological, microtextural and microchemical information is expected to be applicable to other multiple-generation mineral systems and to open new perspectives in understanding the geochronology of metamorphic minerals.
7. The P–T–t evolution of polygenic amphibolites of the Malenco unit was established applying the above criteria to three rocks. They document a double P–T loop between the Triassic and the Cretaceous. The geological evolution corresponding to this P–T–t loop includes a Late Triassic/Early Jurassic decompression from high pressure (and high temperature), exhumation

to the ocean floor in the Late Jurassic, and a Cretaceous reburial, in agreement with known non-isotopic data.

Acknowledgements Field and microprobe work by J.H. and O.M. was supported by SNF grant 20–50454.97/1 to V.T. Isotope research in Bern is partly funded by SNF grant 20–47157.96 to J.D. Kramers Suggestions by Miss U. Casey and M. Bucher are acknowledged. Reviews by G. Féraud, S.P. Kelley and two anonymous referees improved the presentation.

References

Belluso E, Ruffini R, Schaller M, Villa IM (2000) Electron-microscope and Ar isotope characterization of chemically heterogeneous amphiboles from the Palala Shear Zone, Limpopo Belt, South Africa. Eur J Mineral 12: 45–62

Bernoulli D, Winkler W (1990) Heavy mineral assemblages from Upper Cretaceous South- and Austroalpine flysch sequences (N Italy and S Switzerland), source terranes and paleotectonic implications. Eclogae Geol Helv 83: 287–310

Bissig T, Hermann J (1999) From pre-Alpine extension to Alpine convergence: the example of the southwestern margin of the Margna nappe (Val Malenco, N-Italy). Schweiz Mineral Petrogr Mitt 79: 363–380

Boriani AC, Villa IM (1997) Geochronology of regional metamorphism in the Ivrea–Verbano zone and Serie dei Laghi, Italian Alps. Schweiz Mineral Petrogr Mitt 77: 381–401

Bortolotti V, Cellai D, Chiari M, Vaggelli G, Villa IM (1995) $^{40}Ar/^{39}Ar$ dating of Apenninic ophiolites. 3. Plagiogranites from Sasso di Castro sequence, northern Tuscany, Italy. Ofioliti 20: 55–65

Brabander DJ, Giletti BJ (1995) Strontium diffusion kinetics in amphiboles and significance to thermal history determinations. Geochim Cosmochim Acta 59: 2223–2238

Burkhart DJM, O'Neill J (1988) Contrasting serpentinization processes in the Eastern Central Alps. Contrib Mineral Petrol 99: 498–406

Caron M, Dössegger R, Steiger R, Trümpy R (1982) Das Alter der jüngsten Sedimente der Ortler-Decke (Oberostalpin) in der Val Trupchun (Schweizerischer Nationalpark, Graubünden). Eclogae Geol Helv 75: 159–169

Dahl PS (1996a) The effects of composition on retentivity of Ar and O in hornblende and related amphiboles: a field-tested empirical model. Geochim Cosmochim Acta 60: 3687–3700

Dahl PS (1996b) The crystal-chemical basis for Ar retention in micas: inferences from interlayer partitioning and implications for geochronology. Contrib Mineral Petrol 123: 22–39

Desmurs L, Schaltegger U, Manatschal G, Bernoulli D (1999) Geodynamic significance of gabbros along ancient ocean continent transitions. Tasna and Platta nappes, eastern Switzerland. J Conf Abstr 4: 379

Finger W (1978) Die Zone von Samaden (Unterostalpine Decken, Graubünden) und ihre jurassischen Brekzien. PhD Thesis, ETH-Zürich

Foland KA, Fleming TH, Heimann A, Elliot DH (1993) Potassium–argon dating of fine-grained basalts with massive Ar loss: application of the $^{40}Ar/^{39}Ar$ technique to plagioclase and glass from the Kirkpatrick basalt, Antarctica. Chem Geol 107: 173–190

Frey M, Hunziker JC, Frank W, Bocquet J, Dal Piaz GV, Jäger E, Niggli E (1974) Alpine metamorphism of the Alps. A review. Schweiz Mineral Petrogr Mitt 54: 247–290

Froitzheim N, Eberli GP (1990) Extensional detachment faulting in the evolution of a Tethys passive continental margin, Eastern Alps, Switzerland. Geol Soc Am Bull 102: 1297–1308

Furrer H, Aemissegger B, Eberli G, Eichenberger U, Frank S, Naef H, Trümpy R (1985): Field workshop on Triassic and Jurassic sediments in the Eastern Alps of Switzerland. Mitt Geol Inst ETH and Univ Zürich (NF) 248

Guntli P, Liniger M (1989) Metamorphose in der Margna-Decke im Bereich Piz da la Margna und Piz Fedoz (Oberengadin). Schweiz Mineral Petrogr Mitt 69: 289–301

Handy MR, Herwegh M, Kamber BS, Tietz R, Villa IM (1996) Geochronologic, petrologic and kinetic constraints on the evolution of the Err-Platta boundary, part of a fossil continent–ocean suture in the Alps (eastern Switzerland). Schweiz Mineral Petrogr Mitt 76: 453–474

Hansmann W, Hermann J, Müntener O (1996) U–Pb-Datierung des Fedozer Gabbros, einer Intrusion an der Krusten Mantel Grenze. Schweiz Mineral Petrogr Mitt 76: 116–117

Haq BU, Eysinga FWB van (1987) Geological time table, 4th edn. Elsevier, Amsterdam

Hermann J (1997) The Braccia gabbro (Malenco, Alps) Permian intrusion at the crust to mantle interface and Jurassic exhumation during rifting. PhD Thesis, ETH-Zürich, No 12102

Hermann J, Müntener O (1992) Strukturelle Entwicklung im Grenzbereich zwischen dem penninischen Malenco-Ultramafitit und dem Unterostalpin (Margna- und Sella-Decke). Schweiz Mineral Petrogr Mitt 72: 225–240

Hermann J, Müntener O, Trommsdorff V, Hansmann W, Piccardo GB (1997) Fossil crust to mantle transition, Val Malenco (Italian Alps). J Geophys Res 102: 20123–20132

Hohenberg CM, Munk MN, Reynolds JH (1967) Spallation and fissiogenic xenon and krypton from stepwise heating of the Pasamonte achondrite; the case for extinct plutonium 244 in meteorites; relative ages of chondrites and achondrites. J Geophys Res 72: 3139–3177

Kamber BS, Blenkinsop TG, Villa IM, Dahl PS (1995) Proterozoic transpressive deformation in the Northern Marginal Zone, Limpopo Belt, Zimbabwe. J Geol 103: 493–508

Laird J, Albee AL (1981) High pressure metamorphism in mafic schist from northern Vermont. Am J Sci 281: 97–126

Lanphere MA, Dalrymple GB (1976) Identification of excess ^{40}Ar by the $^{40}Ar/^{39}Ar$ age spectrum technique. Earth Planet Sci Lett 32: 141–148

Lee JKW (1993) The argon release mechanisms of hornblende in vacuo. Chem Geol 106: 133–170

Lee JKW, Onstott TC, Cashman KV, Cumbest RJ, Johnson D (1991) Incremental heating of hornblende in vacuo: implications for $^{40}Ar/^{39}Ar$ geochronology and the interpretation of thermal histories. Geology 19: 872–876

Liniger M (1992) Der ostalpin-penninische Grenzbereich im Gebiet der nördlichen Margna-Decke (Graubünden, Schweiz). PhD Thesis, ETH Zürich, No 9769

Livi KJT, Veblen DR (1987) "Eastonite" from Easton, Pennsylvania: a mixture of phlogopite and a new form of serpentine. Am Mineral 72: 113–125

McDougall I, Harrison TM (1988) Geochronology and thermochronology by the $^{40}Ar/^{39}Ar$ method. Oxford University Press, New York

Mellini M, Trommsdorff V, Compagnoni R (1987) Antigorite polysomatism: behaviour during progressive metamorphism. Contrib Mineral Petrol 97: 147–155

Müntener O (1997) The Malenco peridotites (Alps): petrology and geochemistry of subcontinental mantle and Jurassic exhumation during rifting. PhD Thesis, ETH-Zürich, No 12103

Müntener O, Hermann J (1996) The Val Malenco lower crust – upper mantle complex and its field relations (Italian Alps). Schweiz Mineral Petrogr Mitt 76: 475–500

Müntener O, Hermann J, Trommsdorff V (2000) Cooling history and exhumation of lower crustal granulites and upper mantle (Malenco, Eastern Central Alps). J Petrol 41: 175–200

Nyfeler D, Armbruster T, Villa IM (1998) Si, Al, Fe order–disorder in Fe-bearing K-feldspar from Madagascar and its implication to Ar diffusion. Schweiz Mineral Petrogr Mitt 78: 11–21

Onstott TC, Miller ML, Ewing RC, Walsh D (1995) Recoil refinements: implications for the $^{40}Ar/^{39}Ar$ dating technique. Geochim Cosmochim Acta 59: 1821–1834

Parsons I, Brown WL, Smith JV (1999) $^{40}Ar/^{39}Ar$ thermochronology using alkali feldspars: real thermal history or mathematical mirage of microtexture? Contrib Mineral Petrol 136: 92–110

Peretti A (1985) Der Monte-del-Forno-Komplex am Bergell-Ostrand: seine Lithostratigraphie, alpine Tektonik und Metamorphose. Eclogae Geol Helv 78: 23–48

Pouchon JL, Pichoir F (1984) Un nouveau modèle de calcul pour la microanalyse quantitative par spectrométrie de rayons X. I. Application à analyse d' echantillons homogènes. Rech Aérosp 184: 167–192

Pozzorini D, Früh-Green GL (1996) Stable isotope systematics of the Ventina ophicarbonate zone, Bergell contact aureole. Schweiz Mineral Petrogr Mitt 76: 549–564

Raase P (1974) Al and Ti contents of hornblende, indicators of pressure and temperature of regional metamorphism. Contrib Mineral Petrol 45: 231–236

Renne PR, Swisher CC, Deino AL, Karner DB, Owens TL, DePaolo DJ (1998) Intercalibration of standards, absolute ages and uncertainties in $^{40}Ar/^{39}Ar$ dating. Chem Geol 145: 117–152

Spillmann P (1993) Die Geologie des penninisch-ostalpinen Grenzbereichs im südlichen Berninagebirge. PhD Thesis, ETH-Zürich, No 10175

Thöni M, Jagoutz E (1993) Isotopic constraints for eo-Alpine high-P metamorphism in the Austroalpine nappes of the Eastern Alps: bearing on Alpine orogenesis. Schweiz Mineral Petrogr Mitt 73: 177–189

Trommsdorff V, Evans BW (1977) Antigorite ophicarbonates: contact metamorphism in Val Malenco (Italy). Contrib Mineral Petrol 62: 301–312

Trommsdorff V, Piccardo GB, Montrasio A (1993) From magmatism through metamorphism to sea floor emplacement of subcontinental Adria lithosphere during pre-Alpine rifting (Malenco, Italy). Schweiz Mineral Petrogr Mitt 73: 191–203

Turner G, Cadogan P (1974) Possible effects of ^{39}Ar recoil in $^{40}Ar-^{39}Ar$ dating. Proc Lunar Planet Sci Conf 5: 1601–1615

Turner G, Huneke JC, Podosek FA, Wasserburg GJ (1971) $^{40}Ar-^{39}Ar$ ages and cosmic ray exposure ages of Apollo 14 samples. Earth Planet Sci Lett 12: 19–35

Veblen DR (1992) Electron microscopy applied to nonstoichiometry, polysomatism, and replacement reactions in minerals. Rev Mineral 27: 181–229

Villa IM (1997) Direct determination of ^{39}Ar recoil range. Geochim Cosmochim Acta 61: 689–691

Villa IM (1998) Isotopic closure. Terra Nova 10: 42–47

Villa IM (2000) Radiogenic isotopes in fluid inclusions. Lithos (in press)

Villa IM, Ruffini R, Rolfo F, Lombardo B (1996a) Diachronous metamorphism of the Ladakh Terrain at the Karakorum–Nanga Parbat–Haramosh junction (NW Baltistan, Pakistan). Schweiz Mineral Petrogr Mitt 76: 245–264

Villa IM, Grobéty B, Kelley SP, Trigila R, Wieler R (1996b) Assessing Ar transport paths and mechanisms in the McClure Mountains hornblende. Contrib Mineral Petrol 126: 67–80

Villa IM, Ruggieri G, Puxeddu M (1997) Petrology and geochronology of a muscovite–phengite mixture in Larderello–Travale geothermal field (Italy). Eur J Mineral 9: 563–568

Wartho JA, Dodson MH, Rex DC, Guise PG (1991) Mechanisms of Ar release from Himalayan metamorphic hornblende. Am Mineral 76: 1446–1448

Weissert H, Bernoulli D (1985) A transform margin in the Mesozoic Tethys: evidence from the Swiss Alps. Geol Rundsch 74: 655–679